University of Iceland
Faculty of Natural Sciences
Department of Physics

RH-09-99

Finite size effects in the far-infrared absorption of a confined 2DEG

by

Sigurður Ingi Erlingsson

A thesis submitted in partial satisfaction
of the requirements for the degree of Master of
Science in Physics at the University of Iceland

Committee in charge:
Viðar Guðmundsson, Chair
Sven Þ. Sigurðsson

Reykjavík
June 1999

Contents

Chapter 1

Introduction

The motivation for this project was to address some questions on the effects of finite size in systems which have until now only been considered in the limit of infinite size. For example what are the effects of the edge on a finite array of quantum dots and how does a finite length affect the properties of quantum wires.

There has been much effort on the calculations on extended arrays of dots and wires [1, 2, 3, 4] and on single dots and wires [5, 6, 7, 8, 9]. Also of interest is to see how a hard-wall confinement affects quantum dots. Some calculations have been done on such systems, but only for two electrons [10].

From the beginning it was my goal to construct a versatile model which could be used to investigate many types of confined systems, e.g. single dots and wires with different confinement potentials and finite array of dots or wires. Loosely speaking the only limitation is that the wavefunction should have a finite support, but there are also considerations concerning the competing length-scales when a magnetic field is applied.

The main effort of this thesis was to consider size and modulation effects on the absorption spectrum in finite systems. The size was systematically increased and, at the same time, different modulation potential were applied to the system.

Chapter 2

Mesoscopic systems: An introduction

The most convenient way to characterize mesoscopic systems is through the transport behaviour of the electrons. There are two important length scales which determine the transport properties of a conducting sample. First there is the elastic scattering length or mean free path ℓ which is a measure of the average distance travelled by an electron between two scattering impurities in the sample. The phase information of the wavefunction is not lost in these scattering processes, which are independent of temperature. The other scattering mechanism is inelastic scattering caused by lattice vibration and electron-electron interaction. The phase of the wavefunction is lost in these scattering events, which depend on temperature. The average distance travelled between the scattering events is called the phase coherence length ℓ_ϕ.

For low temperatures, when inelastic scatting due to the lattice vibrations is almost frozen out, the coherence length can exceed the sample dimension, or $\ell_\phi \gg L$, where L is the sample size. Under these condition new phenomena such as electron interference can drastically change the transport properties of the sample and Ohms law is no longer applicable. In this regime the electrons can travel through the whole sample without loosing phase coherence. This is the mesoscopic regime [11, 12].

Elastic scattering is independent of temperature simply because the impurities, e.g. substitutional atoms in the lattice, are not temperature dependent (apart form impurity diffusion which is affected by temperature). Thus elastic scattering can only be reduced by reducing the number of impurities in the sample. Furthermore for high purity samples where $\ell \gg L$ one enters the ballistic transport regime where the electrons can travel through the sample without being scattered except at its boundaries.

The key to making mesoscopic samples is micro- or nanofabrication, i.e. the ability to make structures of submicrometer size. In the last two decades manufacturing techniques have allowed dimensions to be reduced and the sample purity increased so that creating a high mobility two dimensional electron gas is possible [13]. Furthermore, systems in one and zero dimensions have also been made. In zero dimensional structures, which are called quantum dots or artificial atoms, the electrons are strongly confined in all directions and, instead of a continuous bandstructure, a discrete energy spectrum is formed.

Using these new devices previous theoretical predictions have been verified and new surprising behaviour has been observed in experiments[1].

2.1 Two dimensional electron gas

The usual starting point for manufacturing systems in reduced dimensions is the two dimensional electron gas (2DEG). This introduction will focus on how the 2DEG is made at the interface of an AlGaAs-GaAs heterojunction.

The high quality samples are grown using molecular beam epitaxy (MBE) which achives atomic layer precision in growing heterogeneous structures. The general scheme for growing the heterostructure is as follows: First a layer of GaAs is grown on a substrate, usually made of GaAs. On top of it a layer of *undoped* $Al_xGa_{1-x}As$ (x is the fraction of Al in the blend) and then a layer of Si doped $Al_xGa_{1-x}As$ is grown, see Fig. 2.1. The Si atoms act as donors for the 2DEG and the undoped layer acts as a barrier between the electrons and the donors to minimize electron scattering by the ionized donors. On top of this a final GaAs layer is grown, a so called cap layer which keeps the Al from oxidizing. Real samples are much more elaborate, commonly a superlattice is grown on the the substrate to improve smoothness of subsequent layers and the Si doping is modulated to maximize mobility [14].

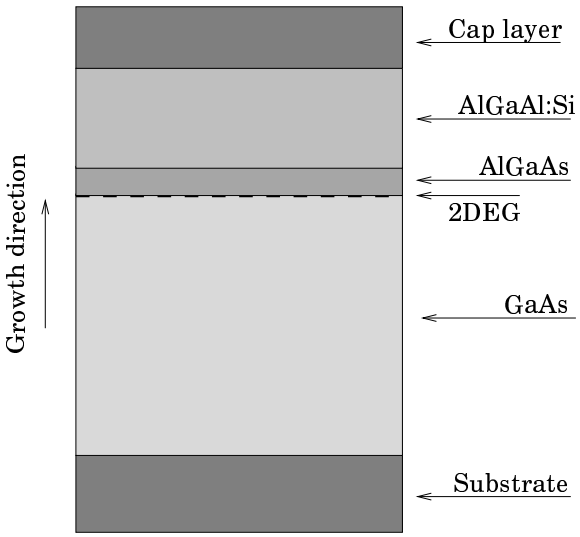

Figure 2.1: A growth sequence for a typical AlGaAs-GaAs heterojunction. At the interface of two substances atomic-layer accuracy is achieved in MBE. The figure is not to scale.

When the GaAs, which is slightly p-doped, comes into contact with the $Al_xGa_{1-x}As$ electron flow across the interface. The flow from the n-doped region into the GaAs is

[1]Nobel prices in physics in 1985 for the IQHE and in 1998 the FQHE

in order to establish an equilibrium charge distribution, which is characterized by a continuous chemical potential across the interface. Equilibrium is reached when the electron flow from the donors is counteracted by the electric field created by the charge transfer across the interface. We assume that the electric field changes smoothly, not affecting the effective mass or bandgaps of the materials. Under these conditions the effect of the electrostatic potential is only a modulation of the band edges as shown in Fig. 2.2. The conduction and valence band edges are denoted by E_c and E_v respectively, $\varepsilon_{\perp,1}$ is the first transverse energy level and μ is the chemical potential.

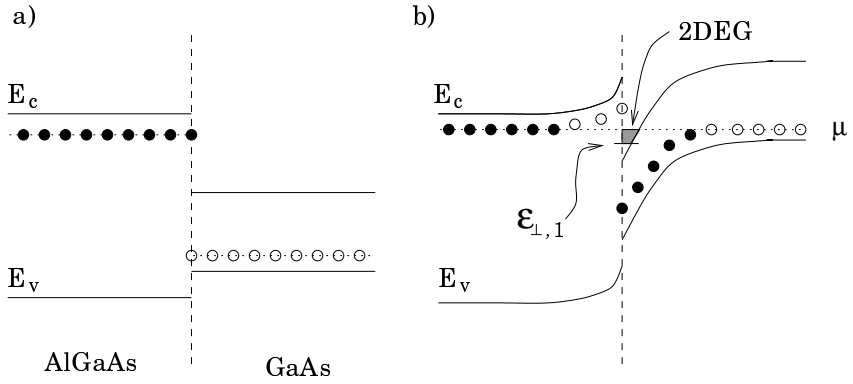

Figure 2.2: Band structure of the heterostructure before and after contact. The chemical potential is fixed and the band edges bend due to the electric potential.

Fig. 2.2a shows the band structure assuming a space-charge neutrality [15] and the effect of the electric potential on the band bending without considering the undoped buffer layer shown in Fig. 2.2b. At the conduction band discontinuity, at the interface, the electrons are 'caught' in a well which can be assumed to be approximately linear in z (the distance from the interface) into the GaAs and infinite in the AlGaAs. The first choice to approximate the eigenfunctions are usually the Airy functions. For more accurate results self-consistent calculations using Fang-Howard wavefunctions is the most popular method [16].

2.2 Lateral potential modulation and confinement

There are several ways of making lateral structures in the 2DEG. The most widely used, and the best controlled, are lithographic methods. These methods are based on either etching or growing lateral patterns on the sample which can influence the distribution of electron in the underlying 2DEG.

In order to grow or etch structures on the sample some sort of a mask has to be placed on it. This mask, or resist, usually consists of a polymer solution with which the sample is coated, e.g. poly-methyl methacryle (PMMA), being the most commonly used resist in nanostructure fabrication [17]. The resist is selectively radiated according

to the pattern desired. When the resist is exposed to the radiation the polymer chains become weaker due to breaking of chemical bonds. After exposure the resist can be removed by immersing it in a solution which does not affect the unradiated part, see Fig. 2.3. Note that this process is similar to photography, just on a smaller scale.

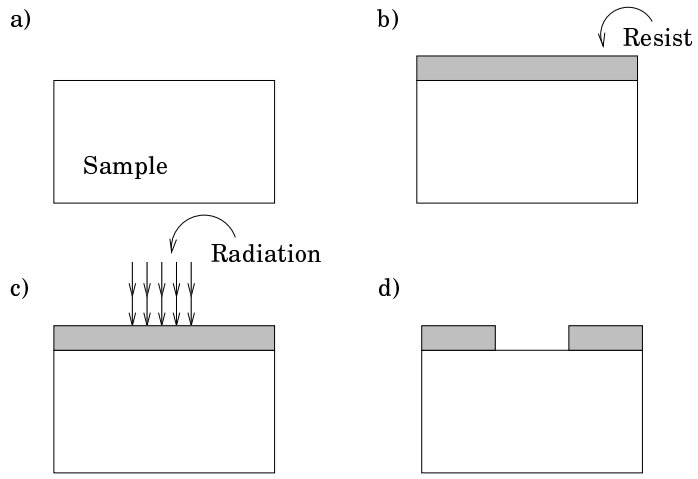

Figure 2.3: Figure (a) shows the clean sample. After the resist has been deposited (b), selective radiation of the resist (c) causes breaking of chemical bonds. Afterwards the sample is 'developed' by immersion in a solvent leaving the unradiated area intact (d).

The resolution of the pattern in the resist depends on the wavelength of the radiation used. For light and UV radiation the highest resolution is $\approx 0.1\,\mu$m, which is the best the industry can achieve today for mass production. To obtain higher resolution for smaller patterns different radiation source has to be used. For a resolution of sub 10 nm electron beams are used to write on the resist.

After the mask (the pattern on the resist) is in place one can proceed either with an additive (growth, evaporation) or subtractive (etching) process to transfer the final pattern onto the sample. Here both cases will be discussed by considering specific examples.

2.2.1 Additive processes

When the mask is ready one can proceed with adding a structure on top of the sample. As an example of a additive process a metal-semiconductor contact depositions will be considered. The metal is evaporated on top of the sample resulting in a layer of metal on the exposed area of the sample and the resist.

If the thickness of the metal is less than the resist, as is shown in Fig. 2.4a, the metal not touching the sample can be removed by lift-off technique. In the lift-off process the sample is immersed in a solution which cleans of the resist and in the process removing all metal which is only attached to the resist.

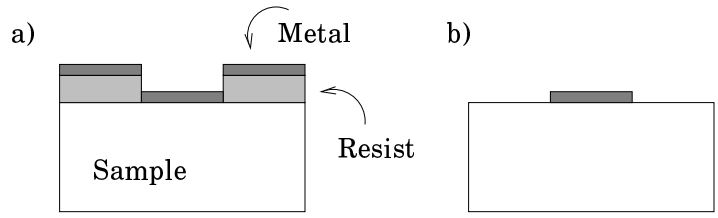

Figure 2.4: A thin metal film is evaporated on the sample (a) and if its thickness is less then that of the resist lift-off can be used to remove the unwanted metal.

When the metal has been deposited it serves as a contact and by applying a negative voltage the electrons below it can be driven off by increasing their potential energy in that region. Depending on the bias either the density is lowered or the 2DEG is totally depleted under the contact.

2.2.2 Subtractive processes

To make an hole or a valley in the sample some sort of solvent is used to etch through the sample. Selective solvent that leaves the resist unaffected, or at least etches it much more slowly than the sample, is chosen. After the desired depth is reached the resist is removed. On this structure further crystal growth can be performed. Etching the

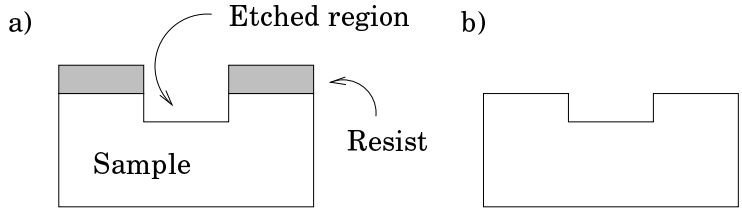

Figure 2.5: A solution that etches the sample material is used to make structures in the sample (a) and after that the resist is removed (b).

samples can be done by using either dry or wet etching. Reactive gases or plasma are used in the dry etching. This method is anisotropic since the etching is in the direction of the ion bombardment. Wet etching uses solvents to make the desired pattern onto the sample. It can be anisotropic because different crystallographic planes have different etch rates.

If the sample in Fig. 2.1 is etched into the donor layer, fewer donors will contribute to the 2DEG in that region, causing a lower density in the 2DEG under the etched area.

2.2.3 A finite array of antidots

Is is possible to etch all the way into the 2DEG, or totally depleting it electrostatically, thus confining it laterally. This also applies to electrostatic depletion. These methods can be used to make a confined 2DEG whose size is such that the lateral energy levels become quantized. It is worth mentioning that etching through the electron gas can introduce edge defects affecting the 2DEG properties.

Finally an atomic force microscope picture of a real sample of a finite array of antidots is shown in Fig. 2.6. This sample was made by etching the AlGaAs donor layer in the region of the black dots [18], i.e. lowering the 2DEG density. The lateral confinement is made by etching into the sample and thus depleting the 2DEG below. The box confinement is not complete in the corners since these are used as contacts for

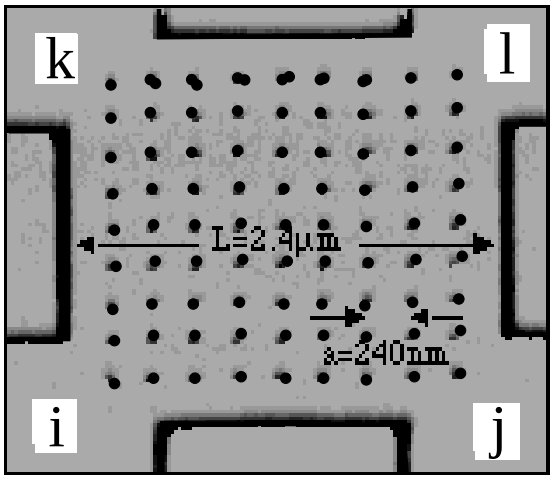

Figure 2.6: An atomic force microscope picture of the antidot sample. The size of the confined region is 2.4 μm and the interdot distance is 240 nm

resistance measurements. Current is passed through contacts i and j and voltage drop from k to l is measured under perpendicular magnetic field. Commensurability effects are seen in the resistance measurements as electrons are 'caught' in pinned orbits that circle one or four dots, depending on the magnetic field, thus increasing the resistance.

Chapter 3

Ground state properties

The system considered consists of electrons at an AlGaAs-GaAs interface. In addition the electrons are confined to a finite region in the plane at the interface. Inside this region there is a modulating potential. The size of this region is such that the lateral energy levels are quantized, opposed to the continuous spectrum of an extended electron gas. How this lateral confinement affects the behaviour of the electrons and how the properties of the system change as the size of the confining region is increased is of interest.

The ground state properties of an electron system are described by the many-body Schrödinger equation. The exact many-body wavefunction is usually not tractable so approximations have to be made. The simplest approximation is to totally ignore the electron-electron interaction, resulting in a single particle spectrum. A better approximation, to be used here, is to include the electron interaction in the Hartree approximation. The Hartree spectrum consists of effective single particle states (Hartree states). From the eigenstates and energies, various properties, e.g. particle density, current density and magnetization are calculated.

3.1 Single particle solution

The Hamiltonian for a single particle includes no term describing the contribution from the electron interaction. It only includes the kinetic operator and the external confining and modulating potential. The potential depends on the structure of the sample and the medium in which the electron is confined.

3.1.1 The Hamiltonian

The single particle Hamiltonian (which is a hermitian operator) for an electron in a magnetic field ($e>0$) and an external potential V_{ext} is given by

$$\begin{aligned} H_0 &= T + V \\ &= \frac{1}{2m^*}(\mathbf{p} + e\mathbf{A}(\mathbf{r}))^2 + V_{\text{ext}}(\mathbf{r}) \\ &= \frac{1}{2m^*}\mathbf{p}^2 + \frac{e^2}{2m^*}\mathbf{A}^2 + \frac{e}{m^*}\mathbf{A}\cdot\mathbf{p} + \frac{e}{2m^*}[\mathbf{p},\mathbf{A}] + V_{\text{ext}}(\mathbf{r}). \end{aligned} \tag{3.1}$$

The effects of the GaAs lattice potential are included in the effective mass m^*. The lattice potential also changes the dielectric constant from the vacuum value ϵ_0 to $\epsilon = \kappa\epsilon_0$. For GaAs the effective electron mass is $m^* = 0.067m_0$ and $\kappa = 12.4$ [19]. Apart from this the lattice potential has almost no effect on the electrons since the Bohr radius a_0^* in GaAs is much larger than the lattice period.

$$\begin{aligned} a_0^* &= \frac{4\pi\epsilon\hbar^2}{m^*e^2} \\ &= \frac{\kappa}{\frac{m^*}{m_0}}a_0 \approx 185\, a_0, \end{aligned}$$

giving $a_0^* = 9.8\,\text{nm}$ compared to the lattice constant $a = 0.57\,\text{nm}$ for GaAs. The wavefunction only 'sees' the average of the lattice potential over many periods, which is approximately constant.

We can assume that at the AlGaAs-GaAs junction the external potential can be separated into perpendicular and parallel parts, with respect to the interface

$$V_{\text{ext}}(\mathbf{r}) = V_{\parallel}(\mathbf{r}_{\parallel}) + V_{\perp}(z). \tag{3.2}$$

The perpendicular potential contains the conduction band structure, shown schematically in Fig. (2.2) which is strongly confining. This confinement is the origin of the 2DEG.

The parallel potential is divided into a confining and a modulating potential

$$V_{\parallel}(\mathbf{r}_{\parallel}) = V_{\text{conf}}(\mathbf{r}_{\parallel}) + V_{\text{mod}}(\mathbf{r}_{\parallel}). \tag{3.3}$$

The lateral confinement causing the system to be finite is chosen to be of a hard-wall type

$$V_{\text{conf}} = \begin{cases} 0 & \text{if } \mathbf{r}_{\parallel} \in \Sigma \\ \infty & \text{otherwise} \end{cases} \tag{3.4}$$

where Σ is some region in the plane of the interface.

The applied magnetic field is constant and perpendicular to the electron gas $\mathbf{B} = B\hat{\mathbf{e}}_z$. The vector potential is chosen to be

$$\mathbf{A}(\mathbf{r}) = \frac{B}{2}\left(-\left(y - \frac{L_y}{2}\right), \left(x - \frac{L_x}{2}\right), 0\right) \tag{3.5}$$

where L_x and L_y are the side lengths in the x and y directions respectively, see Fig. 3.1. This choice of gauge, the symmetric gauge[1] plus a constant term, is convenient due to symmetry reasons which become clear when the matrix elements of the Hamiltonian are calculated, see appendix A.

[1] In the symmetric gauge the vector potential is $\mathbf{A}(\mathbf{r}) = \frac{B}{2}(-y, x, 0)$ [20].

The commutator in eq. (3.1) is zero for this choice of gauge and thus the kinetic term can be separated into parallel and perpendicular parts

$$T = T_{\parallel}(\mathbf{r}_{\parallel}) + T_{\perp}(z).$$

Thus the Shrödinger equation is solved by splitting the Hamiltonian into parallel and perpendicular parts $H_0 = H_{\parallel} + H_{\perp}$ and separating variables. This reduces the problem of solving $H_0\psi = \varepsilon\psi$ to solving two separate equations

$$H_{\parallel}\psi_{\parallel}(\mathbf{r}_{\parallel}) = \varepsilon_{\parallel}\psi_{\parallel}(\mathbf{r}_{\parallel}) \quad \text{and} \quad H_{\perp}\psi_{\perp}(z) = \varepsilon_{\perp}\psi_{\perp}(z). \tag{3.6}$$

The spectrum for the total Hamiltonian is

$$\varepsilon = \varepsilon_{\parallel} + \varepsilon_{\perp} \quad \text{and} \quad \psi(\mathbf{r}) = \psi_{\parallel}(\mathbf{r}_{\parallel})\psi_{\perp}(z). \tag{3.7}$$

Due to the perpendicular confinement the electron gas is very thin, of the order 8-20 nm. This causes large separation between transverse energy levels $\varepsilon_{\perp}$, typically 20-30 eV while the lateral level spacing is of the order of few meV. For normal electron densities and low temperatures only the first transverse level is occupied. To a first approximation, the transverse direction only shifts the lateral energy levels. The wave-function in the transverse direction affects the electron-electron interaction as discussed in section 3.2. Considering these points, a good approximation is to assume that the electron gas has no width and ignore the transverse direction.

Focusing on the lateral Hamiltonian the kinetic operator can be written as

$$\begin{aligned} T_{\parallel} \;= \tfrac{\hbar\omega_c}{2}\Big\{ & -\ell_c^2\left(\tfrac{\partial^2}{\partial x^2} + \tfrac{\partial^2}{\partial y^2}\right) + \left(\left(y - \tfrac{L_y}{2}\right)\tfrac{\partial}{\partial x} - \left(x - \tfrac{L_x}{2}\right)\tfrac{\partial}{\partial y}\right) \\ & + \tfrac{1}{4\ell_c^2}\left(\left(y - \tfrac{L_y}{2}\right)^2 + \left(x - \tfrac{L_x}{2}\right)^2\right)\Big\} \end{aligned} \tag{3.8}$$

introducing the magnetic length $\ell_c^2 = \frac{\hbar}{eB}$ and the cyclotron frequency $\omega_c = \frac{eB}{m^*}$ as the natural length and energy scale respectively. The external potential confines the electrons to a rectangular region

$$\Sigma = \{\mathbf{r}_{\parallel} \mid x \in (0, L_x)\,, y \in (0, L_y)\}\,.$$

The modulating potential in Σ is assumed to be

$$V_{\text{mod}}(\mathbf{r}_{\parallel}) = V_0 \sin^2\left(\frac{M_x \pi x}{L_x}\right)\sin^2\left(\frac{M_y \pi y}{L_y}\right) \tag{3.9}$$

which models an array of quantum dots or antidots depending on the sign of V_0. The number of dots/antidots in the x and y direction is M_x and M_y respectively. The total Hamiltonian for a single electron in Σ is thus

$$H_{\parallel} = T_{\parallel} + V_{\text{mod}}. \tag{3.10}$$

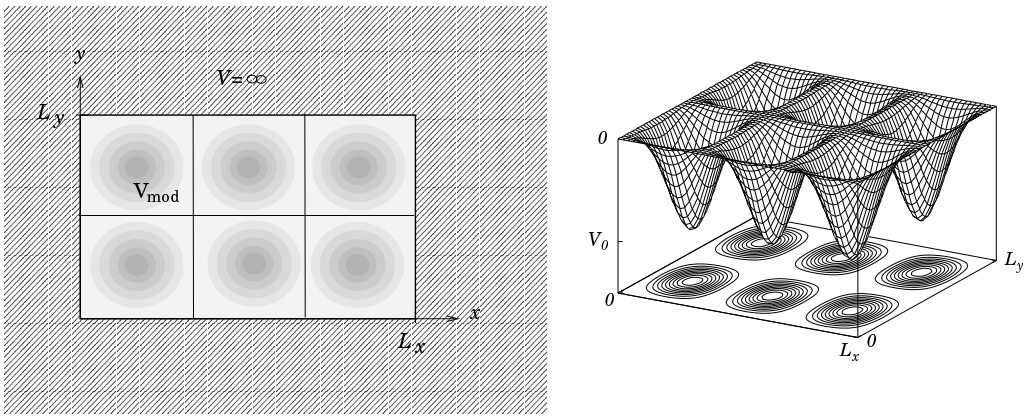

Figure 3.1: The geometry of the system. The left figure shows a schematic potential contour where the hatched region has infinite potential energy. On the right the modulating potential is drawn with $M_x = 3$,$M_y = 2$ and $V_0 < 0$.

3.1.2 The wavefunctions

The electron states of the system are found by solving the Schrödinger equation

$$H\psi = \varepsilon\psi, \tag{3.11}$$

where $H = T_{\|} + V_{\mathrm{mod}}$. This eigenvalue problem and the boundary condition that $\psi = 0$ on $\partial\Sigma$ determine the possible set of solutions. For $B = 0$ and $V_{\mathrm{mod}} = 0$ the Hamiltonian is the two dimensional Laplacian operator whose eigenfunctions are

$$\chi_{mn}(x,y) = \sqrt{\frac{2}{L_x}}\sin\left(\frac{m\pi x}{L_x}\right)\sqrt{\frac{2}{L_y}}\sin\left(\frac{n\pi y}{L_y}\right). \tag{3.12}$$

These functions are used as a basis when solving the general case ($B \neq 0$ and $V_{\mathrm{mod}} \neq 0$) in eq. (3.11), i.e. we write the wavefunctions as

$$\psi(x,y) = \frac{1}{c}\sum_{m',n'=1}^{\infty} c_{m'n'}\sqrt{\frac{2}{L_x}}\sin\left(\frac{m'\pi x}{L_x}\right)\sqrt{\frac{2}{L_y}}\sin\left(\frac{n'\pi y}{L_y}\right) \tag{3.13}$$

where $c = (\sum |c_{m'n'}|^2)^{\frac{1}{2}}$ is the normalization constant.

It is convenient to introduce an inner product of two functions θ and φ on Σ

$$(\varphi,\theta) \equiv \int_{\Sigma} d^2\mathbf{r}_{\|}\varphi^*(\mathbf{r}_{\|})\,\theta(\mathbf{r}_{\|}). \tag{3.14}$$

Taking the inner product of eq. (3.12) and the left hand side of eq. (3.11) one obtains

$$\begin{aligned}(\chi_{mn}, H\psi) &= \frac{1}{c}\sum_{m',n'=1}^{\infty} c_{m'n'}\,(\chi_{mn}, H\chi_{m'n'}) \\ &= \frac{1}{c}\sum_{m',n'=1}^{\infty} c_{m'n'}\,\mathsf{H}_{mn,m'n'}\end{aligned} \tag{3.15}$$

where the matrix elements are defined as

$$\mathsf{H}_{mn,m'n'} = (\chi_{mn}, H\chi_{m'n'}) \tag{3.16}$$

Doing the same for the right hand side of eq. (3.11) and using the fact that there exist bijective maps

$$\ell : (m, n) \to \ell \tag{3.17}$$

one can formally write the Schrödinger equation as the infinite system

$$\begin{bmatrix} \mathsf{H}_{1,1} & & \vdots & & \\ & \ddots & & & \\ \cdots & & \mathsf{H}_{\ell,\ell} & \mathsf{H}_{\ell,\ell+1} & \cdots \\ & & \mathsf{H}_{\ell+1,\ell} & & \\ & & \vdots & & \end{bmatrix} \begin{bmatrix} c_1 \\ \vdots \\ c_\ell \\ c_{\ell+1} \\ \vdots \end{bmatrix} = \varepsilon \begin{bmatrix} c_1 \\ \vdots \\ c_\ell \\ c_{\ell+1} \\ \vdots \end{bmatrix} \tag{3.18}$$

whose eigensolutions are the Fourier coefficients of the corresponding exact eigenfunction of eq. (3.11).

The choice of the sine basis allows the matrix elements to be solved analytically, since the integrals are standard trigonometric integrals. The calculations of the matrix elements are discussed in detail in appendix A.

3.1.3 Diagonalizing a finite matrix

Having transformed the Schrödinger equation into an eigenvector problem we can proceed by solving

$$\mathsf{H}\mathbf{c} = \varepsilon\mathbf{c} \tag{3.19}$$

using standard methods of linear algebra. But first the basis has to be cut to a finite size, i.e. only keeping the first m_{Max} and n_{Max} sine-basis functions in the x and y direction respectively

$$\sum_{m',n'=1}^{\infty} \Rightarrow \sum_{m'=1}^{m_{\text{Max}}} \sum_{n'=1}^{n_{\text{Max}}}.$$

In a $m_{\text{Max}} \times n_{\text{Max}}$ basis for the eigenfunctions eq. (3.13) the eigenvectors have dimension $N = m_{\text{Max}} n_{\text{Max}}$ and the matrix H is $N \times N$. Before constructing the matrix we have to assign to each pair (m, n) a unique integer from 1 to N, to retrieve what mode (m, n) belongs to component c_l after solving eq. (3.19). This is achieved with the mapping

$$\ell(m, n) = m + (n - 1)m_{\text{Max}} \tag{3.20}$$

which has the required properties of

$$\begin{aligned} \ell(1,1) &= 1 \\ \ell(m_{\mathrm{Max}}, n_{\mathrm{Max}}) &= m_{\mathrm{Max}} n_{\mathrm{Max}} = N. \end{aligned}$$

Solving the $N \times N$ eigenvalue problem gives N eigensolutions. The eigenfunctions corresponding to the lowest eigenvalues are better approximations to the correct eigensolutions of the higher eigenvalues. To improve the accuracy the size of the basis is usually chosen to be at least $4\times$ larger than the number of eigensolutions actually needed in the calculations. The size of the total basis, N, is normally between 50 and 500, depending on system size, magnetic field and modulation.

This problem of cutting the basis can be formulated using variational calculations. Using eq. (3.13) and minimizing the Rayleigh quotient

$$\frac{(\psi, H\psi)}{(\psi, \psi)} \tag{3.21}$$

with respect to the c-coefficients we again obtain eq. (3.19). Cutting the basis can thus be viewed as postulating a solution by using a finite sum and minimizing the energy with respect to the truncated subspace.

For $B = 0$ the sine-functions in the Fourier series are eigenfunctions of $T_{\|}$ and, depending on the modulation and the number of particles, the size of the basis can be kept modest. But as the magnetic field is increased the wavefunctions become localized in a region of radius

$$R_c = \ell_c \sqrt{2n+1}, \tag{3.22}$$

where n is the Landau level index. This quantum number is not a 'good' one in this model but as the system size or magnetic field increases Landau levels are formed and the n-index becomes applicable. As R_c gets smaller compared to L_x, L_y the number of coefficients required increases. Also cutting the basis affects higher states in a complex way. Empirically checking the effects of increasing the basis on the spectrum are the best tools to check the accuracy of the eigensolutions.

3.2 Hartree approximation

To model the behaviour of electrons in a realistic manner their mutual interaction has to be included. One way to include the interaction is to postulate effective single particle states from which a specific many body wavefunction is constructed. This is the philosophy of any mean-field theory, like the Hartree-Fock approximation. In this chapter the Hartree-Fock equations are derived be minimizing the total energy of the electrons. Since we are dealing with a two dimensional system a 2D version of the equations will be derived.

In the calculations only the direct term, which is due to electrostatic repulsion of the electrons, is taken into consideration. The direct term is a solution of the Poisson equation for the electron charge density in the system. Finally the Hartree equations are solved. This is non-trivial since the equations are non-linear and have to be solved iteratively in order to apply the standard methods of linear algebra.

3.2.1 Hartree-Fock equations

To accurately model a real system electron interaction has to be included. The natural formalism for this is the many-body Hamiltonian describing a system of N_s electrons in three dimensions [21]

$$H = \sum_{i=1}^{N_s} \left(\frac{\bar{\pi}_i^2}{2m^*} + U(\mathbf{r}_i) \right) + \frac{1}{2} \sum_{i \neq j=1}^{N_s} \frac{e^2}{4\pi\epsilon |\mathbf{r}_i - \mathbf{r}_j|}, \tag{3.23}$$

where the generalized momentum $\bar{\pi}_i = \mathbf{p}_i + e\mathbf{A}$ of particle i has been introduced. The potential U contains the external potential and the electrostatic potential caused by background charges. These charges are ionized donors which ensure charge neutrality. The many-body Schrödinger equation is given as

$$H\Psi = \mathcal{E}\Psi, \tag{3.24}$$

where the wavefunction including all the electrons is

$$\Psi = \Psi(\mathbf{r}_1 s_1, \mathbf{r}_2 s_2, \ldots, \mathbf{r}_{N_s} s_{N_s}) \tag{3.25}$$

with spatial coordinates $\mathbf{r}_i$ and spin s_i. Although the Hamiltonian H is not spin dependent the wavefunction has to contain spin indices for correct symmetry properties.

Solving eq. (3.24) exactly is not possible except for few particles using numerically exact diagonalization [7]. To solve the equation[2] some sort of approximations and assumptions about the structure of the wavefunction have to be made. In the Hartree-Fock approximation the wavefunction is assumed to be of the form

$$\Psi = \frac{1}{\sqrt{N_s!}} \det[\phi_i(\mathbf{r}_j s_j)] \tag{3.26}$$

$$= \frac{1}{\sqrt{N_s!}} \begin{vmatrix} \phi_1(\mathbf{r}_1 s_1) & \phi_1(\mathbf{r}_2 s_2) & \ldots & \phi_1(\mathbf{r}_{N_s} s_{N_s}) \\ \phi_2(\mathbf{r}_1 s_1) & \phi_2(\mathbf{r}_2 s_2) & \ldots & \phi_2(\mathbf{r}_{N_s} s_{N_s}) \\ \vdots & \vdots & & \vdots \\ \phi_{N_s}(\mathbf{r}_1 s_1) & \phi_{N_s}(\mathbf{r}_2 s_2) & \ldots & \phi_{N_s}(\mathbf{r}_{N_s} s_{N_s}) \end{vmatrix}, \tag{3.27}$$

which is antisymmetric under particle interchange. The single particle wavefunctions are solutions of

$$H_{\mathrm{HF}} \phi_i(\mathbf{r}s) = \varepsilon_i \phi_i(\mathbf{r}s), \tag{3.28}$$

[2] These calculations follow the approach used in [22].

but $H_{\rm HF}$ is not known. To derive the Hartree-Fock single particle potential one minimizes the total energy of the system, assuming the many-body wavefunction is given by the Slater-determinant of single particle wavefunctions. The problem is thus solving the variational equation

$$\frac{\partial}{\partial\phi^*_\alpha(x)}\left[\langle\Psi|H|\Psi\rangle - \sum_{i=1}^{N_s}\varepsilon_i\int dy\phi^*_i(y)\phi_i(y)\right] = 0 \tag{3.29}$$

with Lagrange multipliers ε_i and introducing the generic coordinate $x = (\mathbf{r}, s)$.

Previous equation contained a functional derivative. Before proceeding we shall consider a short introduction to functional derivatives. Consider a functional $F[J(t)]$. The functional derivative of F with respect to J is defined as

$$\frac{\partial F[J(\tau)]}{\partial J(t)} \equiv \lim_{\epsilon\to 0}\frac{F[J(\tau)+\epsilon\delta(\tau-t)] - F[J(\tau)]}{\epsilon}.$$

Now looking at the functional $F[J(t)] = \int d\tau f(\tau)J(\tau)$ the derivative becomes

$$\begin{aligned}\frac{\partial F[J(\tau)]}{\partial J(t)} &= \lim_{\epsilon\to 0}\frac{\int f(\tau)(J(\tau)+\epsilon\delta(\tau-t)) - \int f(\tau)J(\tau)}{\epsilon}\\ &= f(t)\end{aligned} \tag{3.30}$$

To simplify the notation in the following equations a generic two particle potential $v(x,x') = v(x',x)$ is used to represent the Coulomb interaction. The definition of the functional derivative can be applied to eq. (3.29)

$$\begin{aligned}\frac{\partial}{\partial\phi^*_\alpha(x)}\Bigg[&\sum_{i=1}^{N_s}\int dy\phi^*_i(y)\left(\frac{\bar\pi^2}{2m^*}+U(y)\right)\phi_i(y)\\ &+\frac{1}{2}\sum_{i,j=1}^{N_s}\int dydy'\phi^*_i(y)\phi^*_j(y')v(y,y')\phi_i(y)\phi_j(y')\\ &-\frac{1}{2}\sum_{i,j=1}^{N_s}\int dydy'\phi^*_i(y)\phi^*_j(y')v(y,y')\phi_j(y)\phi_i(y')\\ &-\sum_{i=1}^{N_s}\varepsilon_i\int dy\phi^*_i(y)\phi_i(y)\Bigg]\end{aligned} \tag{3.31}$$

$$\begin{aligned}= &\overbrace{\left(\frac{\bar\pi^2}{2m^*}+U(x)\right)}^{H_0}\phi_\alpha(x) + \sum_{i=1}^{N_s}\int dy\phi^*_i(y)v(x,y)\phi_i(y)\phi_\alpha(x)\\ &-\sum_{i=1}^{N_s}\int dy\phi^*_i(y)v(x,y)\phi_i(x)\phi_\alpha(y) - \varepsilon_i\phi_\alpha(x) = 0.\end{aligned} \tag{3.32}$$

The derivatives of the double integrals[3] give two terms which can be added, after a

[3]This is the same as when a product of functions is differentiated or $(fg)' = f'g + g'f$

change of variables $y' \to y$ and dummy indices $j \to i$. This is the reason for the disappearance of the factor $\frac{1}{2}$.

The sum over the first N_s states is due to a zero temperature. For $T = 0$ the states with lowest energy are occupied and the Pauli exclusion principle ensures that only one electron resides in each state. Defining the quantities

$$\rho(y) = \sum_{i=1}^{N_s} \phi_i^*(y)\phi_i(y) \qquad \text{and} \qquad \rho(x,y) = \sum_{i=1}^{N_s} \phi_i^*(y)\phi_i(x) \tag{3.33}$$

as the density and the density matrix respectively the Hartree-Fock equations become

$$\left[H_0 + \int dy \rho(y) v(x,y)\right] \phi_\alpha(x) - \int dy \rho(x,y) v(x,y) \phi_\alpha(x) = \varepsilon \phi_\alpha(x). \tag{3.34}$$

For $T \neq 0$ some states above the Fermi level are partially occupied. How these states are occupied is described by the Fermi distribution $f(\varepsilon_i - \mu)$ where μ is the chemical potential ensuring the correct number of particles

$$N_s = \sum_{i=1}^{\infty} f(\varepsilon_i - \mu). \tag{3.35}$$

The sums in the eq. (3.33) change when non-zero temperature is included

$$\sum_{i=1}^{N_s} \Rightarrow \sum_{i=1}^{\infty} f(\varepsilon_i - \mu) \equiv \sum_{i=1}^{\infty} f_i \,, \tag{3.36}$$

where the sum is performed over all states.

When changing from the generic variable $x = (\mathbf{r}, s)$ one has to remember that $\int dy$ includes a sum over spin states. Since each state is assumed to be an eigenstate of $\hat{s}_z$ eq. (3.34) can be written as

$$\begin{aligned} &H_0\phi_i(\mathbf{r}) + \int d^3\mathbf{r}' \sum_{i'} f_{i'} \frac{e^2 \phi_{i'}^*(\mathbf{r}')\phi_{i'}(\mathbf{r}')}{4\pi\epsilon|\mathbf{r}' - \mathbf{r}|}\phi_i(\mathbf{r}) \\ &- \int d^3\mathbf{r}' \sum_{i'} f_{i'} \delta_{s_{i'} s_i} \frac{e^2 \phi_{i'}^*(\mathbf{r}')\phi_{i'}(\mathbf{r})}{4\pi\epsilon|\mathbf{r}' - \mathbf{r}|}\phi_i(\mathbf{r}') = \varepsilon_i \phi_i(\mathbf{r}). \end{aligned} \tag{3.37}$$

The former term containing the interaction is called the direct term and the latter the exchange term. Here exchange refers to the exchange of the quantum numbers $\phi_{i'}(\mathbf{r}')\phi_i(\mathbf{r}) \to \phi_{i'}(\mathbf{r})\phi_i(\mathbf{r}')$.

3.2.2 Hartree-Fock equations in two dimensions

How does the strong confinement affect the Hartree-Fock approximation ? We split the single particle Hamiltonian into parallel and perpendicular parts $H_0 = H_\parallel + H_\perp$ and write the eigenfunctions as

$$\phi_i(\mathbf{r}) = \varphi_m(\mathbf{r}_\parallel) u_n(z) \tag{3.38}$$

where $i = (m, n)$ are the 'quantum numbers' in the lateral and transverse directions. Using this separation but retaining the index i for the spins one can write eq. (3.37) as

$$\begin{aligned}
& u_n(z) H_\parallel \varphi_m(\mathbf{r}_\parallel) + \varphi_m(\mathbf{r}_\parallel) H_\perp u_n(z) \\
+ & \int d^2\mathbf{r}'_\parallel dz' \sum_{m'n'} f_{m'n'} \frac{e^2 \varphi^*_{m'}(\mathbf{r}'_\parallel) u^*_{n'}(z') \varphi_{m'}(\mathbf{r}'_\parallel) u_{n'}(z')}{4\pi\epsilon \sqrt{(\mathbf{r}'_\parallel - \mathbf{r}_\parallel)^2 + (z'-z)^2}} \varphi_m(\mathbf{r}_\parallel) u_n(z) \\
- & \int d^2\mathbf{r}'_\parallel dz' \sum_{m'n'} f_{m'n'} \delta_{s_{i'} s_i} \frac{e^2 \varphi^*_{m'}(\mathbf{r}'_\parallel) u^*_{n'}(z') \varphi_{m'}(\mathbf{r}_\parallel) u_{n'}(z)}{4\pi\epsilon \sqrt{(\mathbf{r}'_\parallel - \mathbf{r}_\parallel)^2 + (z'-z)^2}} \varphi_m(\mathbf{r}'_\parallel) u_n(z') \\
= & \ \varepsilon_{mn} \varphi_m(\mathbf{r}_\parallel) u_n(z). \qquad (3.39)
\end{aligned}$$

Assuming a sufficiently strong confinement in the z direction so that only the first transverse state is occupied $n' = 1$ and neglecting interactions with higher states ($n > 1$) one can put both $n = n' = 1$ and rewrite last equation as

$$\begin{aligned}
& u_1(z) H_\parallel \varphi_m(\mathbf{r}_\parallel) + \varphi_m(\mathbf{r}_\parallel) H_\perp u_1(z) \\
+ & \int d^2\mathbf{r}'_\parallel \sum_{m'} f_{m'1} \varphi^*_{m'}(\mathbf{r}'_\parallel) \varphi_{m'}(\mathbf{r}'_\parallel) \int dz' \frac{e^2 |u_1(z')|^2}{4\pi\epsilon \sqrt{(\mathbf{r}'_\parallel - \mathbf{r}_\parallel)^2 + (z'-z)^2}} \varphi_m(\mathbf{r}_\parallel) u_1(z) \\
- & \int d^2\mathbf{r}'_\parallel \sum_{m'} f_{m'1} \delta_{s_{i'} s_i} \varphi^*_{m'}(\mathbf{r}'_\parallel) \varphi_{m'}(\mathbf{r}_\parallel) \int dz' \frac{e^2 |u_1(z')|^2}{4\pi\epsilon \sqrt{(\mathbf{r}'_\parallel - \mathbf{r}_\parallel)^2 + (z'-z)^2}} \varphi_m(\mathbf{r}'_\parallel) u_1(z) \\
= & \ \varepsilon_{m1} \varphi_m(\mathbf{r}_\parallel) u_1(z). \qquad (3.40)
\end{aligned}$$

The strong confinement localizes the wavefunctions in the $z = 0$ plane and the z'-integration is performed noting that the eigenfunctions are assumed to be normalized

$$\begin{aligned}
\int dz' & \frac{e^2 |u_1(z')|^2}{4\pi\epsilon \sqrt{(\mathbf{r}'_\parallel - \mathbf{r}_\parallel)^2 + (z'-z)^2}} \\
& \approx \frac{e^2}{4\pi\epsilon \sqrt{(\mathbf{r}'_\parallel - \mathbf{r}_\parallel)^2 + z^2}}. \qquad (3.41)
\end{aligned}$$

This result is exact for a perfect 2DEG where $|u_1(z)|^2 = \delta(z)$ but in other cases, if the function $|u_1|^2$ is localized around $z = 0$, eq. (3.41) may also apply to a high accuracy. Using this result and dividing eq. (3.40) by $u_1(z)$ and taking the limit $z \to 0$ one arrives

at the Hartree-Fock for the two dimensional system

$$\begin{aligned} H_\parallel\varphi_m(\mathbf{r}_\parallel) &+ \int d^2\mathbf{r}'_\parallel \sum_{m'} f_{m'} \frac{e^2\varphi^*_{m'}(\mathbf{r}'_\parallel)\varphi_{m'}(\mathbf{r}'_\parallel)}{4\pi\epsilon|\mathbf{r}'_\parallel - \mathbf{r}_\parallel|}\varphi_m(\mathbf{r}_\parallel) \\ &- \int d^2\mathbf{r}'_\parallel \sum_{m'} f_{m'}\delta_{s_{m'}s_m} \frac{e^2\varphi^*_{m'}(\mathbf{r}'_\parallel)\varphi_{m'}(\mathbf{r}_\parallel)}{4\pi\epsilon|\mathbf{r}'_\parallel - \mathbf{r}_\parallel|}\varphi_m(\mathbf{r}'_\parallel) \\ = H_\parallel\varphi_m(\mathbf{r}_\parallel) &+ \int d^2\mathbf{r}'_\parallel \frac{e^2\rho(\mathbf{r}'_\parallel)}{4\pi\epsilon|\mathbf{r}'_\parallel - \mathbf{r}_\parallel|}\varphi_m(\mathbf{r}_\parallel) \\ &- \int d^2\mathbf{r}'_\parallel \sum_{m'} f_{m'}\delta_{s_{m'}s_m} \frac{e^2\varphi^*_{m'}(\mathbf{r}'_\parallel)\varphi_{m'}(\mathbf{r}_\parallel)}{4\pi\epsilon|\mathbf{r}'_\parallel - \mathbf{r}_\parallel|}\varphi_m(\mathbf{r}'_\parallel) \\ &= (\varepsilon_m - \varepsilon_{\perp,1})\varphi_m(\mathbf{r}_\parallel) \end{aligned} \tag{3.42}$$

where the transverse part is defined as

$$\varepsilon_{\perp,1} = \lim_{z\to 0}\frac{H_\perp u_1(z)}{u_1(z)} \tag{3.43}$$

and $\rho(\mathbf{r}_\parallel)$ is the particle density. The transverse wavefunctions do not enter the Hartree-Fock terms so that u_1 is an eigenfunction of $H_\perp$. The transverse part only causes a shift in the zero on the lateral energy scale, which will be ignored in the calculations. This result is only valid for a perfect 2DEG. All references to the transverse quantum number n have been ignored and the index m is used to replace i. For quasi 2D systems where $|u_1(z)|^2 \neq \delta(z)$ the above equations are still a reasonable approximation as long as eq. (3.41) is 'valid', in some sense, and if not other forms of the Coulomb interaction can be used.

3.2.3 The Poisson equation

As was mentioned earlier the potential U in eq. (3.23) contains the interaction of the electrons with the positive background. Assuming that the potential can be written as

$$U(\mathbf{r}) = V_{\text{ext}}(\mathbf{r}) + \int d^2\mathbf{r}'_\parallel \frac{-e^2\frac{N_s}{L_xL_y}}{4\pi\epsilon|\mathbf{r}'_\parallel - \mathbf{r}_\parallel|}, \tag{3.44}$$

where $\frac{N_s}{L_xL_y}$ is the donor density and the contribution of the donors is separated from external contributions, see eq. (3.2). The donor interaction and the direct term in eq. (3.42) are of the same type and can be combined into one equation. The Hartree potential V_H is a solution of the Poisson equation [23]

$$\nabla^2 V_H = -\frac{e^2}{\epsilon}n(\mathbf{r}_\parallel)\delta(z), \tag{3.45}$$

where n is the total charge density of the system

$$-en(\mathbf{r}_\parallel) = -e\left(\rho(\mathbf{r}_\parallel) - \frac{N_s}{L_x L_y}\right). \tag{3.46}$$

The electron density ρ is the same as in eq. (3.33) and the constant term on the right side represents the positive background. Eq. (3.44) assumes that the donors are in the plane of the 2DEG which is not the case for real samples.

The solution of eq. (3.45) can be written on integral form as

$$V_H(\mathbf{r}_\parallel) = \int d^2\mathbf{r}'_\parallel \frac{e^2 n(\mathbf{r}'_\parallel)}{4\pi\epsilon|\mathbf{r}'_\parallel - \mathbf{r}_\parallel|}. \tag{3.47}$$

This integral cannot be solved analytically and when the Hartree matrix elements have to be evaluated four dimensional numerical integration over Σ has to be performed $(m_{\mathrm{Max}} n_{\mathrm{Max}})^2$-times. To avoid these lengthy numerical calculations we assume that the Hartree potential can be written in the region Σ as

$$V_H(\mathbf{r}_\parallel, 0) = \sum_{m',n'=0} \tilde{\sigma}_{m'}\tilde{\sigma}_{n'} V_{H,m'n'} \cos\left(\frac{m'\pi x}{L_x}\right)\cos\left(\frac{n'\pi y}{L_y}\right), \tag{3.48}$$

where the terms are weighted according to $\tilde{\sigma}_m = 1 - \frac{1}{2}\delta_{0,m}$. This form is not necessary and other ones can be used, e.g. sum over orthogonal polynomials, as long as the matrix elements can be evaluated analytically.

The expansion coefficients are obtained using their definition, in this case

$$V_{H,mn} = \frac{2^2}{L_x L_y}\int_\Sigma d^2\mathbf{r}_\parallel V_H(\mathbf{r}_\parallel, 0)\cos\left(\frac{m\pi x}{L_x}\right)\cos\left(\frac{n\pi y}{L_y}\right), \tag{3.49}$$

and by solving eq. (3.45) in the Fourier space. Transforming the Poisson equation we have

$$-k^2 V_H = -\frac{e^2}{\epsilon} n(\mathbf{k}_\parallel). \tag{3.50}$$

The right hand side does not contain k_z so the inverse Fourier transform in k_z can be performed. Using residual calculus the Hartree potential in $\mathbf{k}_\parallel$ is

$$V_H(\mathbf{k}_\parallel, z) = \frac{e^2}{2\epsilon} n(\mathbf{k}_\parallel)\frac{\mathrm{e}^{-k_\parallel|z|}}{k_\parallel}. \tag{3.51}$$

Thus, putting $z = 0$ because we are only interested in the potential at the 2DEG, we have by the inverse transform that

$$V_H(\mathbf{r}_\parallel, 0) = \left(\frac{e^2}{4\pi\epsilon L}\right)\frac{L}{2\pi}\int d^2\mathbf{k}_\parallel \frac{n(\mathbf{k}_\parallel)}{k_\parallel}\mathrm{e}^{-i\mathbf{r}_\parallel\cdot\mathbf{k}_\parallel}, \tag{3.52}$$

where the characteristic length of the system is $L = \sqrt{L_x L_y}$. This equation is inserted into eq. (3.49) and the $\mathbf{r}_\parallel$ integration is performed analytically giving

$$V_{H,mn} = V_{\text{Coul}} \frac{L}{2\pi} \int d^2\mathbf{k}_\parallel \frac{n(\mathbf{k}_\parallel)}{k_\parallel} I_m(k_x L_x) I_n(k_y L_y), \tag{3.53}$$

where the 'Coulomb energy' as $V_{\text{Coul}} = e^2/4\pi\epsilon L$. The function I_m is defined as

$$I_m(x) = 2 \int_0^1 du \cos(m\pi u) e^{ixu}. \tag{3.54}$$

Only the $\mathbf{k}_\parallel$ integration remains and the positive background in eq. (3.46) ensures that $n(\mathbf{k}_\parallel)/k_\parallel$ is defined for $\mathbf{k}_\parallel = 0$. The functions I_m are known analytically and the two dimensional integral in eq. (3.53) is easy to implement using Gaussian integration on a subdivided integration region.

Since the number of $V_{H,mn}$ coefficients is always less than $(m_{\text{Max}} n_{\text{Max}})^2$ this method is much more efficient and transparent than the method involving the four dimensional integration.

3.2.4 Solving the Hartree equations

In summary the results of the previous sections can be combined into the two dimensional Hartree equations

$$(H + V_{\text{H}}(\mathbf{r}_\parallel))\varphi_i(\mathbf{r}_\parallel) = \varepsilon_i \varphi_i(\mathbf{r}_\parallel). \tag{3.55}$$

The lateral part of the Hamiltonian is the same as in eq. (3.10) and the in-plane Hartree potential is described by eq. (3.48).

These equations are non-linear since the Hartree potential contains the density, i.e. the potential is a functional of all the solutions

$$V_H(\mathbf{r}_\parallel) = V_H[\{\varphi_i\}_i](\mathbf{r}_\parallel). \tag{3.56}$$

This causes some problems when solving the equations. Here an iterative method is used to solve them. One starts with a set of wavefunctions which is used to calculate the Hartree potential. Then eq. (3.55) is solved using the method in section 3.1.2 to obtain a new set of solutions. This process is continued until the change in the solutions is less than some tolerance δ. One usually starts with a set of non-interacting solutions and continues from there. Assuming that a solution exists this process may converge. In reality this is not the case. Strong oscillations occur in the solutions which often overshoot the 'equilibrium' solutions. This effect can be avoided if the Hartree potential is turned on slowly or adiabatically. Instead of using the full Hartree potential a mixture of the current and previous is used according to

$$\tilde{V}_{\text{H}}^{[k]} = \lambda V_{\text{H}}^{[k]} + (1-\lambda)\tilde{V}_{\text{H}}^{[k-1]}, \tag{3.57}$$

where $\lambda \in (0,1)$ is the mixing parameter and $[k]$ is the iteration number. The tolerance is defined as the relative difference in the Hartree potential between two loops, see the flowchart in Fig. (3.2). It is usually chosen between $10^{-3} - 10^{-2}$. The convergence is normally quite fast and higher values of the mixing parameter converge faster, as long as oscillations are avoided.

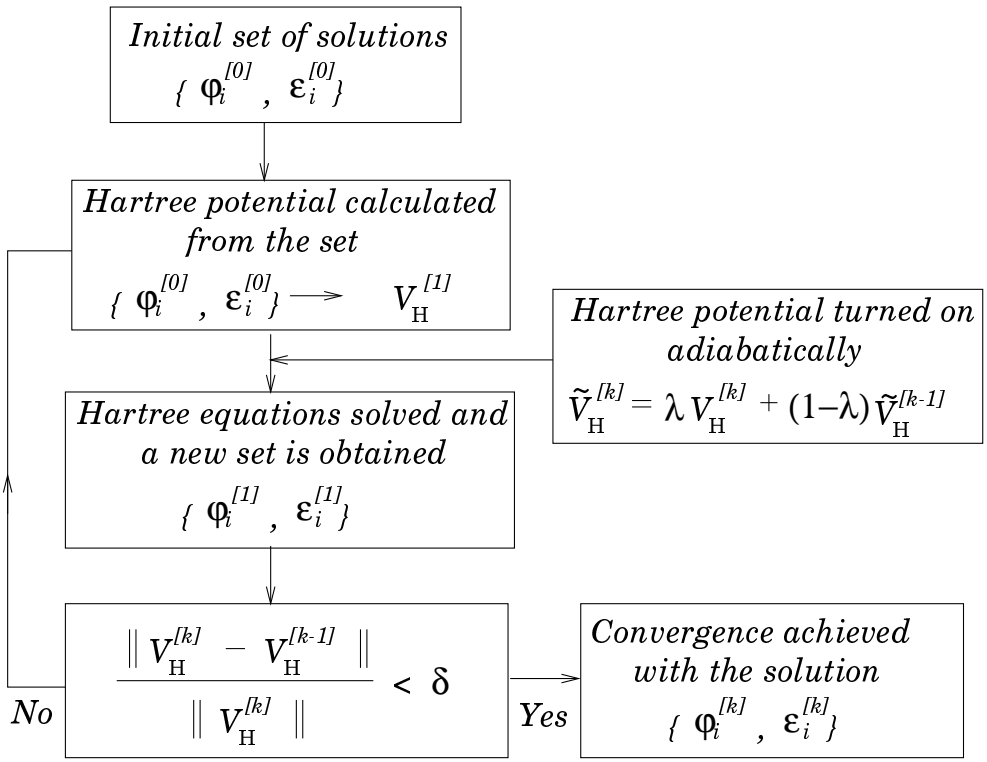

Figure 3.2: Flow chart for the Hartree iteration.

Chapter 4

FIR absorption

Far-infrared absorption spectroscopy is a convenient way to probe the energy structure of mesoscopic systems. It has been used to study homogeneous and modulated 2DEGs, quantum dots and wires both by calculations and with experiments [24, 8]. Here the absorption spectra are calculated using a self-consistent field approximation.

The density response function of the system is derived using the density operator after its basic properties have been discussed. Then the self-consistent field is calculated and the equations describing the absorption are derived. Finally resonances in the total field and the absorption spectra are discussed and compared.

4.1 The density operator in linear approximation

The density operator is defined in such a way that its many body expectation value yields the particle density. Letting n denote the particle density we can write this in the following way

$$n(\mathbf{r}) = \langle \Psi | \bar{\rho}(\mathbf{r}) | \Psi \rangle. \tag{4.1}$$

For $T = 0$ the first N_s single particle states are occupied with probability 1 and all other states are unoccupied. In this case the density operator is defined by [22]

$$\bar{\rho}(\mathbf{r}) = \sum_{i=1}^{N_s} \delta(\mathbf{r} - \mathbf{r}_i). \tag{4.2}$$

The delta functions can be interpreted as the probability of finding the particle at $\mathbf{r}$ if it is at $\mathbf{r}_i$. In the case of a single particle the sum is replaced by one term which yields the normal equation for the density $n = \psi^* \psi$.

For a Hartree type many body wavefunction, which is the product of the single

particle states, eq. (4.1) can be written, using the Dirac notation, as

$$\begin{aligned} n(\mathbf{r}) &= \langle\Psi|\sum_{i=1}^{N_s}\delta(\mathbf{r}-\mathbf{r}_i)|\Psi\rangle \\ &= \sum_{i=1}^{N_s}\langle\phi_i|\delta(\mathbf{r}-\mathbf{r}_i)|\phi_i\rangle \\ &= \sum_{i=1}^{\infty}\langle\phi_i|\hat{\rho}\delta(\mathbf{r}-\mathbf{r}_i)|\phi_i\rangle \\ &= \mathrm{tr}\{\hat{\rho}\delta(\mathbf{r}-\mathbf{r}')\}. \end{aligned} \tag{4.3}$$

In the third step a probability, or statistical operator $\hat{\rho}$, was introduced which ensures the correct occupation of the states, thus the finite sum can be replaced with a sum over all states. The sum is just the trace over single particle states, which is a well known result [25]. The many body information is contained in the trace and the statistical operator so that the variable $\mathbf{r}_i$ can be replaced by an arbitrary $\mathbf{r}'$. Eq. (4.3) can be formulated for non-zero temperatures where the temperature enters the statistical operator $\hat{\rho} = \hat{\rho}(T)$. For equilibrium situations the statistical operator is given by

$$\hat{\rho}_0 = f(H-\mu), \tag{4.4}$$

where f is the Fermi distribution.

The equation of motion for the statistical operator is given by

$$\frac{d}{dt}\hat{\rho}(t) = \frac{1}{i\hbar}[H,\hat{\rho}]. \tag{4.5}$$

The effect of adding a small perturbation $\delta V(t)$ to the equilibrium hamiltonian H_0 on the density operator can be calculated by linearizing the equation of motion. First the operators are divided into the equilibrium and a perturbed part

$$\begin{aligned} H(t) &= H_0 + \delta V(t) \\ \hat{\rho}(t) &= \hat{\rho}_0 + \delta\hat{\rho}(t). \end{aligned} \tag{4.6}$$

The external perturbing potential is assumed to be harmonic and turned on adiabatically so that $H = H_0$ when $t \to -\infty$. This is done by including a factor $e^{\eta t}$ in the perturbing potential, where $\eta \to 0^+$. The adiabatic factor is necessary since it is not enough to assume that the perturbation is 'small' because an infinitesimal perturbation acting for a long enough time can change the ground state [26]. In that case it is no longer valid to speak of a perturbation of the ground state since it may have completely changed.

Because the unperturbed wavefunctions are simultaneous eigenfunctions of H_0 and $\hat{\rho}_0$ one can obtain the matrix elements of $\delta\hat{\rho}$. Using the Fourier transform of the

linearized equation of motion eq. (4.5) the matrix elements of the statistical operator can be written as

$$\delta\hat{\rho}_{\alpha\beta}(\omega) = \frac{n_\beta - n_\alpha}{\hbar\omega - \hbar\omega_{\alpha\beta} + i\hbar\eta}\delta V_{\alpha\beta}(\omega), \tag{4.7}$$

where $\omega_{\alpha\beta} = (\varepsilon_\alpha - \varepsilon_\beta)/\hbar$, and $n_\alpha = f(\varepsilon_\alpha - \mu)$ is the occupation of state α, i.e. $\hat{\rho}_0|\alpha\rangle = n_\alpha|\alpha\rangle$.

The matrix element of the statistical operator can be used to calculate the induced density. Inserting the perturbation part into eq. (4.3) we otains the induced density

$$\begin{aligned}
\delta n(\mathbf{r},\omega) &= \mathrm{tr}\{\delta(\mathbf{r}-\mathbf{r}')\delta\hat{\rho}\} \\
&= \sum_{\alpha\beta}\psi_\alpha(\mathbf{r})\psi^*_\beta(\mathbf{r})\delta\hat{\rho}_{\alpha\beta}(\omega) \\
&= \int d^3\mathbf{r}'\left(\sum_{\alpha\beta}\psi_\alpha(\mathbf{r})\psi^*_\beta(\mathbf{r})\frac{n_\beta - n_\alpha}{\hbar\omega - \hbar\omega_{\alpha\beta} + i\hbar\eta}\psi^*_\alpha(\mathbf{r}')\psi_\beta(\mathbf{r}')\right)\delta V(\mathbf{r}',\omega) \\
&\equiv \int d^3\mathbf{r}' D(\mathbf{r},\mathbf{r}',\omega)\delta V(\mathbf{r}',\omega),
\end{aligned} \tag{4.8}$$

which defines the density response function $D(\mathbf{r},\mathbf{r}',\omega)$. The integral comes from the matrix element of the perturbing potential. Eq. (4.8) relates the perturbing potential to the density change through equilibrium state quantities only, which is the hallmark of linear response. The intensity of the perturbation is irrelevant since all effects scale linearly in the perturbation.

4.2 The self-consistent field approximation

The basic philosophy of the self-consistent field approximation is that the total field, not just the external field, is used to calculate the induced field. When an external field is applied to a system of charges they tend to rearrange themselves in order to screen it. The total, self consistent field (SCF) is the sum of the external field ϕ_{ext} and the induced one ϕ_{ind} caused by the charge movement. The induced field is a functional of the SCF ϕ_{sc}, thus the self-consistent scheme for the fields becomes

$$\phi_{\mathrm{sc}}(\mathbf{r},t) = \phi_{\mathrm{ext}}(\mathbf{r},t) + \phi_{\mathrm{ind}}[\phi_{\mathrm{sc}}](\mathbf{r},t). \tag{4.9}$$

Since we are interested in the response to FIR radiation with the wavelength $\lambda = 2\pi c/\omega \gg \lambda_F$, where λ_F is the Fermi wavelength, the retardation effects can be ignored. The electrons manage to keep up with the external field and no phase difference develops between ϕ_{ext} and ϕ_{ind} in the time domain. For a plane wave external field

$$\phi_{\mathrm{ext}}(\mathbf{r},t) = \phi_{\mathrm{ext},0}e^{-i(\mathbf{r}_\parallel\cdot\mathbf{k}_{\parallel,0}-\omega t)} \tag{4.10}$$

the time dependence of the terms in eq. (4.9) is harmonic

$$\phi(\mathbf{r},t) = \phi(\mathbf{r},\omega)e^{i\omega t}. \tag{4.11}$$

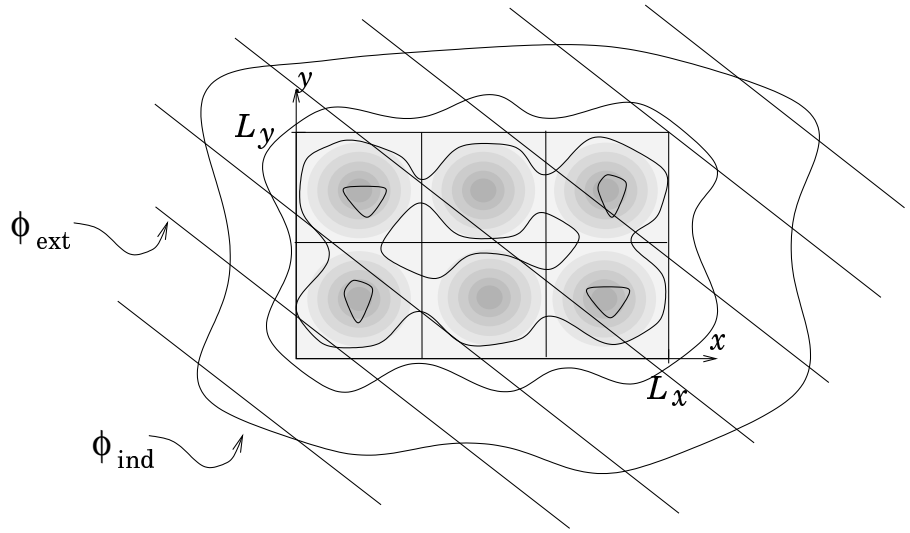

Figure 4.1: The field lines for the external and the induced field are shown schematically around the system. Close to the system the induced field is strong but decays sharply as we move away from the system.

The induced field is given by Poisson's equation

$$\nabla^2\phi_{\rm ind}[\phi_{\rm sc}](\mathbf{r},\omega) = \frac{e}{\epsilon}\delta n[\phi_{\rm sc}](\mathbf{r},\omega), \tag{4.12}$$

which has the well known solution [23]

$$\begin{aligned}
\phi_{\rm ind}(\mathbf{r},\omega) &= -\frac{e}{4\pi\epsilon}\int d^3\mathbf{r}'\frac{\delta n(\mathbf{r}',\omega)}{|\mathbf{r}-\mathbf{r}'|} \\
&= -\frac{e}{4\pi\epsilon}\int d^2\mathbf{r}'_\parallel dz'\frac{\delta n(\mathbf{r}'_\parallel,z',\omega)}{|(\mathbf{r}_\parallel,z)-(\mathbf{r}'_\parallel,z')|} \\
&= -\frac{e}{4\pi\epsilon}\int d^2\mathbf{r}'_\parallel dz'\frac{\delta n(\mathbf{r}'_\parallel,\omega)\delta(z')}{|(\mathbf{r}_\parallel,z)-(\mathbf{r}'_\parallel,z')|} \\
&= -\frac{e}{4\pi\epsilon}\int d^2\mathbf{r}'_\parallel\frac{\delta n(\mathbf{r}'_\parallel,\omega)}{\sqrt{(\mathbf{r}_\parallel-\mathbf{r}'_\parallel)^2+z^2}}.
\end{aligned} \tag{4.13}$$

Here the z-dependence of the particle density of the 2DES is assumed to be of the form

$$\delta n(\mathbf{r}_\parallel,z,\omega) = \delta n(\mathbf{r}_\parallel,\omega)\delta(z),$$

and thus the induced field is a convolution of the particle density

$$\delta n(\mathbf{r}_\parallel, \omega)$$

and the Coulomb potential

$$-\frac{e}{4\pi\epsilon}\frac{1}{\sqrt{\mathbf{r}_\parallel^2 + z^2}}.$$

When all calculations on the z variable have been performed the limit $z \to 0$ is taken and all quantities will be $\mathbf{r}_\parallel$-dependent, i.e. a two dimensional system will remain.

4.2.1 The SCF in k-space

The quantities of interest are those which can be conveniently compared with experimental results. For this reason it is convenient to work in **k**-space, which is the Fourier transform of the corresponding quantity in **r**-space. The $\mathbf{k}_\parallel$ and ω dependent quantities can then be compared to the wavenumber and frequency results of spectroscopic experiments. The Fourier transform of the induced field is given by

$$\phi_{\mathrm{ind}}(\mathbf{k}_\parallel, \omega) = \delta n(\mathbf{k}_\parallel, \omega)\left(-\frac{e}{4\pi\epsilon}\right) 2\pi \frac{e^{-k_\parallel z}}{k_\parallel}$$

and the problem is shifted to finding the Fourier transform of the induced particle density $\delta n(\mathbf{k}_\parallel, \omega)$.

The SCF induces a density change through the density response function $D(\mathbf{r}, \mathbf{r}', \omega)$ which relates the induced density to the local perturbing field felt by the charges

$$\begin{aligned}
\delta n(\mathbf{r}, \omega) &= \int d^3\mathbf{r}' D(\mathbf{r}, \mathbf{r}', \omega)\left(-e\phi_{\mathrm{sc}}(\mathbf{r}', \omega)\right) \\
&= \int d^2\mathbf{r}_\parallel dz' D(\mathbf{r}_\parallel, \mathbf{r}'_\parallel, \omega)\delta(z)\delta(z')\left(-e\phi_{\mathrm{sc}}(\mathbf{r}'_\parallel, z', \omega)\right) \\
&= \delta(z)\int d^2\mathbf{r}'_\parallel D(\mathbf{r}_\parallel, \mathbf{r}'_\parallel, \omega)\left(-e\phi_{\mathrm{sc}}(\mathbf{r}'_\parallel, 0, \omega)\right) \\
&= \delta(z)\,\delta n(\mathbf{r}_\parallel, \omega). \qquad (4.14)
\end{aligned}$$

The important property of the response function

$$D(\mathbf{r}, \mathbf{r}', \omega) = D(\mathbf{r}_\parallel, \mathbf{r}'_\parallel, \omega)\delta(z)\delta(z') \qquad (4.15)$$

is obvious when the two dimensionality of the system is considered. The response function gives the 'effect' at $\mathbf{r}$ which is caused at $\mathbf{r}'$. Since there are only charges at $z' = 0$ that can cause change and response can only occur when the charges are at $z = 0$ the δ-functions are justified.

The Fourier transform of the density is thus

$$\begin{aligned}
\delta n(\mathbf{k}_\parallel,\omega) &= \int d^2\mathbf{r}_\parallel d^2\mathbf{r}'_\parallel e^{i\mathbf{k}_\parallel\cdot\mathbf{r}_\parallel} D(\mathbf{r}_\parallel,\mathbf{r}'_\parallel,\omega)\left(-e\phi_{\rm sc}(\mathbf{r}'_\parallel,0,\omega)\right)\\
&= \int d^2\mathbf{r}_\parallel d^2\mathbf{r}'_\parallel d^2\mathbf{q}_\parallel e^{i\mathbf{k}_\parallel\cdot\mathbf{r}_\parallel}\\
&\qquad \times D(\mathbf{r}_\parallel,\mathbf{r}'_\parallel,\omega)\frac{1}{(2\pi)^2}e^{-i\mathbf{q}_\parallel\cdot\mathbf{r}'_\parallel}\left(-e\phi_{\rm sc}(\mathbf{q}_\parallel,0,\omega)\right)\\
&= \int d^2\mathbf{q}_\parallel D(\mathbf{k}_\parallel,\mathbf{q}_\parallel,\omega)\left(-e\phi_{\rm sc}(\mathbf{q}_\parallel,0,\omega)\right), \qquad (4.16)
\end{aligned}$$

where the 'Fourier transform' of the response function is defined as

$$D(\mathbf{k}_\parallel,\mathbf{q}_\parallel,\omega)=\frac{1}{(2\pi)^2}\int d^2\mathbf{r}_\parallel d^2\mathbf{r}'_\parallel e^{i\mathbf{k}_\parallel\cdot\mathbf{r}_\parallel}D(\mathbf{r}_\parallel,\mathbf{r}'_\parallel,\omega)e^{-i\mathbf{q}_\parallel\cdot\mathbf{r}'_\parallel}. \qquad (4.17)$$

From this equation an integral equation in $\phi_{\rm sc}$ can be derived (for now the z,ω dependence in the fields is suppressed but note that $\phi_{\rm sc}$ in the integral only depends on $z=0$)

$$\begin{aligned}
\phi_{\rm sc}(\mathbf{k}_\parallel) &= \phi_{\rm ext}(\mathbf{k}_\parallel)+\left(-\frac{e}{4\pi\epsilon}\right)2\pi\frac{e^{-k_\parallel z}}{k_\parallel}\int d^2\mathbf{q}_\parallel D(\mathbf{k}_\parallel,\mathbf{q}_\parallel,\omega)\left(-e\phi_{\rm sc}(\mathbf{q}_\parallel)\right)\\
&= \phi_{\rm ext}(\mathbf{k}_\parallel)+\frac{e^2}{2\epsilon}\frac{e^{-k_\parallel z}}{k_\parallel}\int d^2\mathbf{q}_\parallel D(\mathbf{k}_\parallel,\mathbf{q}_\parallel,\omega)\phi_{\rm sc}(\mathbf{q}_\parallel)\\
&= \phi_{\rm ext}(\mathbf{k}_\parallel)+\int d^2\mathbf{q}_\parallel K(\mathbf{k}_\parallel,\mathbf{q}_\parallel;z,\omega)\phi_{\rm sc}(\mathbf{q}_\parallel), \qquad (4.18)
\end{aligned}$$

where an integral kernel has been introduced

$$K(\mathbf{k}_\parallel,\mathbf{q}_\parallel;z,\omega)=\frac{e^2}{2\epsilon}\frac{e^{-k_\parallel z}}{k_\parallel}D(\mathbf{k}_\parallel,\mathbf{q}_\parallel,\omega). \qquad (4.19)$$

The SCF $\phi_{\rm sc}$ is thus represented by an integral equation. Before solving it the behaviour of the kernel $K(\mathbf{k}_\parallel,\mathbf{q}_\parallel;z,\omega)$ will be investigated.

4.2.2 The density response and the integral kernel

Restating the results of linear response in section 4.1 the particle density response function can be written as

$$\begin{aligned}
D(\mathbf{r}_\parallel,\mathbf{r}'_\parallel,\omega) &= \sum_{\alpha\,\beta}\frac{n_\beta-n_\alpha}{\hbar\omega-\hbar\omega_{\alpha\beta}+i\hbar\eta}\varphi_\alpha(\mathbf{r}_\parallel)\varphi^*_\beta(\mathbf{r}_\parallel)\varphi^*_\alpha(\mathbf{r}'_\parallel)\varphi_\beta(\mathbf{r}'_\parallel)\\
&\equiv \sum_{\alpha\,\beta}\tilde{n}_{\alpha\beta}(\omega)\varphi_\alpha(\mathbf{r}_\parallel)\varphi^*_\beta(\mathbf{r}_\parallel)\varphi^*_\alpha(\mathbf{r}'_\parallel)\varphi_\beta(\mathbf{r}'_\parallel) \qquad (4.20)
\end{aligned}$$

where the φ's are the eigenfunctions of the interacting non-perturbed system. Inserting the eigenfunctions of eq. (3.13) into the Fourier transform of the response function we get

$$\begin{aligned} D(\mathbf{r}_\parallel, \mathbf{r}'_\parallel, \omega) &= \frac{1}{(2\pi)^2} \sum_{\alpha\,\beta} \tilde{n}_{\alpha\beta}(\omega) \int d^2\mathbf{r}_\parallel e^{i\mathbf{k}_\parallel \cdot \mathbf{r}_\parallel} \varphi_\alpha(\mathbf{r}_\parallel) \varphi^*_\beta(\mathbf{r}_\parallel) \\ &\qquad \times \int d^2\mathbf{r}'_\parallel e^{-i\mathbf{q}_\parallel \cdot \mathbf{r}'_\parallel} \varphi^*_\alpha(\mathbf{r}'_\parallel) \varphi_\beta(\mathbf{r}'_\parallel) \\ &\equiv \frac{1}{(2\pi)^2} \sum_{\alpha\,\beta} \tilde{n}_{\alpha\beta}(\omega) d_{\alpha\beta}(\mathbf{k}_\parallel)\, d^*_{\alpha\beta}(\mathbf{q}_\parallel). \end{aligned} \tag{4.21}$$

Equation (4.19) relates the density response to the kernel

$$\begin{aligned} K(\mathbf{r}_\parallel, \mathbf{r}'_\parallel, \omega) &= \frac{e^2}{2\epsilon} \frac{1}{k_\parallel} \frac{1}{(2\pi)^2} \sum_{\alpha\,\beta} \tilde{n}_{\alpha\beta}(\omega) d_{\alpha\beta}(\mathbf{k}_\parallel)\, d^*_{\alpha\beta}(\mathbf{q}_\parallel) \\ &= V_{\mathrm{Coul}} \frac{L}{2\pi} \sum_{\alpha\,\beta} \tilde{n}_{\alpha\beta}(\omega) \frac{d_{\alpha\beta}(\mathbf{k}_\parallel)}{k_\parallel} d^*_{\alpha\beta}(\mathbf{q}_\parallel), \end{aligned} \tag{4.22}$$

where L and V_{Coul} are defined in eqs. (3.52) and (3.53). A kernel of this kind, where each term in the sum separate in $\mathbf{k}_\parallel$ and $\mathbf{q}_\parallel$, is called degenerate. This separation of variables is a result of the rectangular confinement which allows the use of Cartesian coordinates in the problem. This proves to be very helpful when it comes to solving the integral equation for ϕ_{sc}.

4.2.3 Solving the SCF integral equation

Now that the basic equation for the SCF has been developed we can proceed to solve it. The field is described by an integral equation with a degenerate kernel, the integral equation can be transformed into an algebraic equation [27]. Since we are only interested in the SCF for the 2DEG putting $z = 0$ simplifies the integral equation, which becomes

$$\begin{aligned} \phi_{\mathrm{sc}}(\mathbf{k}_\parallel) &= \phi_{\mathrm{ext}}(\mathbf{k}_\parallel) + \int d^2\mathbf{q}_\parallel K(\mathbf{k}_\parallel, \mathbf{q}_\parallel; 0, \omega) \phi_{\mathrm{sc}}(\mathbf{q}_\parallel) \\ &= \phi_{\mathrm{ext}}(\mathbf{k}_\parallel) + V_{\mathrm{Coul}} \frac{L}{2\pi} \sum_{\alpha\,\beta} \tilde{n}_{\alpha\beta}(\omega) \frac{d_{\alpha\beta}(\mathbf{k}_\parallel)}{k_\parallel} \int d^2\mathbf{q}_\parallel d^*_{\alpha\beta}(\mathbf{q}_\parallel) \phi_{\mathrm{sc}}(\mathbf{q}_\parallel) \\ &\equiv \phi_{\mathrm{ext}}(\mathbf{k}_\parallel) + V_{\mathrm{Coul}} \frac{L}{2\pi} \sum_{\alpha\,\beta} \tilde{n}_{\alpha\beta}(\omega) \frac{d_{\alpha\beta}(\mathbf{k}_\parallel)}{k_\parallel} \frac{x_{\alpha\beta}}{L^2}. \end{aligned} \tag{4.23}$$

Note that $V_{\mathrm{Coul}}\tilde{n}_{\alpha\beta}$ is a dimensionless quantity. The terms $x_{\alpha\beta}$ introduced here are expansion coefficients for the SCF given by

$$x_{\alpha\beta} = L^2 \int d^2\mathbf{q}_\parallel d^*_{\alpha\beta}(\mathbf{q}_\parallel) \phi_{\mathrm{sc}}(\mathbf{q}_\parallel). \tag{4.24}$$

Using the definition for the inverse Fourier transform it is easy to show that $x_{\alpha\beta} = 2\pi(\psi_\alpha, \phi_{\rm sc}\psi_\beta)$ which are just the matrix elements of the SCF.

The dimension of the matrix element $x_{\alpha\beta}$ is the same as that of the field since the $d_{\alpha\beta}$-functions are dimensionless. These coefficients are determined in a self-consistent manner by inserting eq. (4.23) into (4.24). This gives a set of algebraic equations for the x's

$$\begin{aligned} x_{\alpha\beta} &= L^2 \int d^2\mathbf{q}_\parallel d^*_{\alpha\beta}(\mathbf{q}_\parallel)\Big\{ \phi_{\rm ext}(\mathbf{q}_\parallel) \\ &\qquad + V_{\rm Coul}\frac{L}{2\pi}\sum_{\alpha'\,\beta'}\tilde{n}_{\alpha\beta}(\omega)\frac{d_{\alpha'\beta'}(\mathbf{q}_\parallel)}{q_\parallel}\frac{x_{\alpha'\beta'}}{L^2}\Big\} \\ &= L^2 \int d^2\mathbf{q}_\parallel d^*_{\alpha\beta}(\mathbf{q}_\parallel)\phi_{\rm ext}(\mathbf{q}_\parallel) \\ &\quad + V_{\rm Coul}\sum_{\alpha'\,\beta'}\tilde{n}_{\alpha\beta}(\omega)\left\{\frac{L}{2\pi}\int d^2\mathbf{q}_\parallel d^*_{\alpha\beta}(\mathbf{q}_\parallel)\frac{1}{q_\parallel}d_{\alpha'\beta'}(\mathbf{q}_\parallel)\right\}x_{\alpha'\beta'} \qquad (4.25) \\ &= L^2 \int d^2\mathbf{q}_\parallel d^*_{\alpha\beta}(\mathbf{q}_\parallel)\phi_{\rm ext}(\mathbf{q}_\parallel) + V_{\rm Coul}\sum_{\alpha'\,\beta'}\tilde{n}_{\alpha\beta}(\omega)\hat{\mathsf{A}}_{\alpha\beta,\alpha'\beta'}\,x_{\alpha'\beta'} \\ &= b_{\alpha\beta} + \sum_{\alpha'\,\beta'}\mathsf{A}(\omega)_{\alpha\beta,\alpha'\beta'}\,x_{\alpha'\beta'}. \qquad (4.26) \end{aligned}$$

The last equation shows how the $x_{\alpha\beta}$'s depend on ω through $\mathsf{A}(\omega)$. The integral in eq. (4.25) is independent of ω which will prove important because the most computationally intensive calculation involves finding the A matrix elements. Due to the discrete energy levels, ω is independent of $\mathbf{k}$ and thus the A matrix elements need only to be calculated once. To simplify the notation a new index $\alpha\beta \to i$ is used and the matrix form of eq. (4.26) can be written as

$$\sum_{i'}(\delta_{ii'} - \mathsf{A}(\omega)_{ii'})x_{i'} = b_i \qquad (4.27)$$

or in matrix form

$$(\mathsf{I} - \mathsf{A}(\omega))\mathbf{x} = \mathbf{b}. \qquad (4.28)$$

Solving this equation gives the induced field in eq. (4.23) caused by a specific 'external field' $\mathbf{b}$. The magnitude of the induced field is an indication of how strongly the charges are affected. This last equation can be compared to the usual electrostatic equation

$$(1 + \chi)\phi_{\rm tot} = \phi_{\rm ext}. \qquad (4.29)$$

If one ignores that A is a matrix , it can be interpreted as the electric susceptibility χ which indicates how much the medium is polarized. Furthermore the matrix A contains

the depolarization shift, i.e. the deviation of the absorption energy from the energy level differences [28, 29], caused by the non-constant perturbing field[1].

It is interesting to look at whether there exist solutions of eq. (4.28) for $\mathbf{b} = 0$, i.e. what are the eigenmodes of the system? The sufficient condition for $(\mathsf{I} - \mathsf{A}(\omega))\mathbf{x} = \mathbf{0}$ is that

$$\det(\mathsf{I} - \mathsf{A}(\omega)) = 0. \tag{4.30}$$

This is the well known condition for the existence of longitudinal waves (plasmon) in an electron gas, i.e. $\epsilon(\omega) = 0$ [30].

4.2.4 The induced density

For a given system there can be many eigenmodes which satisfy eq. (4.30). The origin of these resonances are not always known beforehand. In order to identify what kind of charge movement is excited the induced density can be a valuable tool. For example

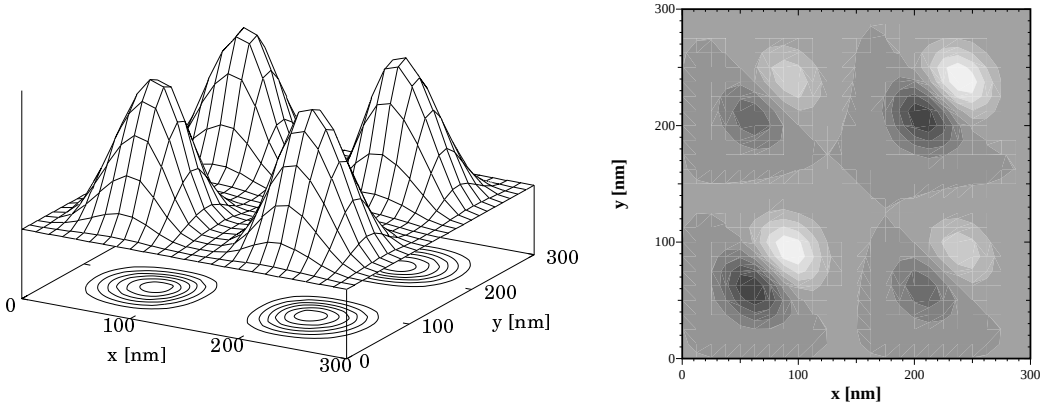

Figure 4.2: The ground state density, to the left, and a contour plot of the induced density for the 3×3 system for $V_0 = -10\,\mathrm{meV}$ modulation at $B = 0\,\mathrm{T}$.

the structure of the induced density can tell whether the charges of the system are moving in 'unison' or if an internal charge motion is taking place. The non-resonant frequencies give a zero induced density, which means that charge motion can not be excited at that frequency. As an example we consider a 2×2 array of dots. The side lengths are $L_x = L_y = 300\,\mathrm{nm}$ and the modulation is $V_0 = -10\,\mathrm{meV}$. The wave vector lies along the diagonal. The left figure in Fig. 4.2 shows the equilibrium density where the isolated dots can be seen and the induced density, figure to the right, shows charge oscillations in each dot. The edge limits the charge motion and forces the induced density to be zero at the boundary giving a standing wave-like motion.

[1] Compare this to Fermi's golden rule where the field is assumed to be constant in space and thus the transition rate contains a delta function $\delta(\hbar\omega - (\varepsilon_\alpha - \varepsilon_\beta))$

4.3 The power absorption

The current that is induced in the system has to lie in the plane of the 2DEG. Thus the current density vector has only non-zero lateral components. The induced current is related to the total electric field through the conductivity tensor

$$\begin{aligned} \mathbf{J}(\mathbf{r}) &= \delta(z)\mathbf{J}_{\parallel}(\mathbf{r}_{\parallel}) \\ &= \delta(z)\int d^2\mathbf{r}'_{\parallel}\hat{\sigma}(\mathbf{r}_{\parallel},\mathbf{r}'_{\parallel})\mathbf{E}_{\mathrm{sc}\,\parallel}(\mathbf{r}'), \end{aligned} \tag{4.31}$$

which is a non-local version of Ohm's law. The conductivity tensor is written as a 2×2 matrix so that only the lateral components of the total field $\mathbf{E}_{\parallel\,\mathrm{sc}}(\mathbf{r}')$ couple to the in-plane current.

The power absorbed in the system can be calculated as Joule heating[2] of the electrons. The total field interacts with the induced current resulting in a power loss

$$P = \frac{1}{2}\int d^3\mathbf{r}'\Re\{\mathbf{J}(\mathbf{r}')\cdot\mathbf{E}^*_{\mathrm{sc}\,\parallel}(\mathbf{r}'_{\parallel})\}. \tag{4.32}$$

The factor $\frac{1}{2}$ is due to the time average over the harmonic fields. Compared to eq. (4.30) which contains all possible transitions the power absorption predominantly shows the collective, many body transitions. Using the definition of the inverse Fourier transform the power absorption can be written as

$$P = \frac{1}{2}\frac{1}{(2\pi)^2}\int d^2\mathbf{k}_{\parallel}\Re\{\mathbf{J}_{\parallel}(\mathbf{k}_{\parallel})\cdot\mathbf{E}^*_{\mathrm{sc}\,\parallel}(\mathbf{k}_{\parallel})\}. \tag{4.33}$$

Inserting Ohm's law into this equation and using the same formalism as in eqs. (4.16) and (4.17) for the conductivity tensor, we obtain a new equation for the absorption

$$\begin{aligned} P &= \frac{1}{2}\frac{1}{(2\pi)^2}\int d^2\mathbf{k}_{\parallel}d^2\mathbf{q}_{\parallel}\Re\{\hat{\sigma}(\mathbf{k}_{\parallel},\mathbf{q}_{\parallel})(i\mathbf{q}_{\parallel}\phi_{\mathrm{sc}}(\mathbf{q}_{\parallel}))\cdot(-i\mathbf{k}_{\parallel}\phi^*_{\mathrm{sc}}(\mathbf{k}_{\parallel}))\} \\ &= \frac{1}{2}\frac{1}{(2\pi)^2}\int d^2\mathbf{k}_{\parallel}d^2\mathbf{q}_{\parallel}\Re\{(-i)\phi^*_{\mathrm{sc}}(\mathbf{k}_{\parallel})(i\mathbf{k}_{\parallel}\cdot\hat{\sigma}(\mathbf{k}_{\parallel},\mathbf{q}_{\parallel})\mathbf{q}_{\parallel})\phi_{\mathrm{sc}}(\mathbf{q}_{\parallel})\} \\ &= \frac{1}{2}\frac{1}{(2\pi)^2}\int d^2\mathbf{k}_{\parallel}d^2\mathbf{q}_{\parallel}\Re\{(-i)\phi^*_{\mathrm{sc}}(\mathbf{k}_{\parallel})\left(\frac{k_{\parallel}\omega}{2\pi}\epsilon(\mathbf{k}_{\parallel},\mathbf{q}_{\parallel})-\delta(\mathbf{k}_{\parallel}-\mathbf{q}_{\parallel})\right)\phi_{\mathrm{sc}}(\mathbf{q}_{\parallel})\} \\ &= \frac{1}{2}\frac{\omega}{(2\pi)^3}\int d^2\mathbf{k}_{\parallel}\Re\{(-i)k_{\parallel}\phi^*_{\mathrm{sc}}(\mathbf{k}_{\parallel})(\phi_{\mathrm{ext}}(\mathbf{k}_{\parallel})-\phi_{\mathrm{sc}}(\mathbf{k}_{\parallel}))\}. \end{aligned} \tag{4.34}$$

In the third step a relationship connecting $\hat{\sigma}$ and ϵ was used. This relation is derived in appendix B. The definitions

$$\begin{aligned} \phi_{\mathrm{ext}}(\mathbf{k}_{\parallel}) &\equiv \int d^2\mathbf{q}_{\parallel}\,\epsilon(\mathbf{k}_{\parallel},\mathbf{q}_{\parallel})\phi_{\mathrm{sc}}(\mathbf{q}_{\parallel}) \\ \phi_{\mathrm{sc}}(\mathbf{k}_{\parallel}) &= \int d^2\mathbf{q}_{\parallel}\,\delta(\mathbf{k}_{\parallel}-\mathbf{q}_{\parallel})\phi_{\mathrm{sc}}(\mathbf{q}_{\parallel}) \end{aligned} \tag{4.35}$$

[2]The surrounding medium absorbs all the heat generated keeping the temperature constant.

were used in the last line of eq. (4.34). Now the final steps can be performed which give

$$\begin{aligned} P &= \frac{1}{2}\frac{\omega}{(2\pi)^3}\int d^2\mathbf{k}_\parallel \Re\{(-i)k_\parallel \phi^*_{\rm sc}(\mathbf{k}_\parallel)\phi_{\rm ext}(\mathbf{k}_\parallel) + ik_\parallel|\phi_{\rm sc}(\mathbf{k}_\parallel)|^2\} \\ &= \frac{1}{2}\frac{\omega}{(2\pi)^3}\int d^2\mathbf{k}_\parallel \Re\{(-i)k_\parallel \phi^*_{\rm sc}(\mathbf{k}_\parallel)\phi_{\rm ext}(\mathbf{k}_\parallel)\} \\ &= -\frac{1}{2}\frac{\omega}{(2\pi)^3}\int d^2\mathbf{k}_\parallel \Im\{k_\parallel \phi^*_{\rm sc}(\mathbf{k}_\parallel)\phi_{\rm ext}(\mathbf{k}_\parallel)\}. \end{aligned} \tag{4.36}$$

For the plane wave external field in eq. (4.10) the Fourier transform is delta function at $\mathbf{k}_\parallel = \mathbf{k}_{\parallel,0}$. In this case the integral in eq. (4.36) is readily evaluated and the power absorbed is proportional to $\Im\{\phi^*_{\rm sc}(\mathbf{k}_{\parallel,0})\}$.

4.4 Comparing the absorption and eigenmodes in $\phi_{\rm ind}$

The kernel in the integral equation used to solve for the SCF includes the density response function, as seen in eq. (4.22). The density response function contains a sum over all transitions between different states, which means that the SCF has contributions from all possible transitions. The determinant of the matrix in eq. (4.28) can be interpreted as a dielectric function of the electrons. The zeros of this function represent transitions in the system and the slope at the zero identifies their type [31, 32].

In the power spectra collective excitations are dominant and single particle transitions have low oscillator strength. Since Joule heating is used to define the absorption only transition which transfer energy from the electric field to the electrons can contribute to the spectrum [26].

Comparing these two methods the absorption has obvious advantages over the determinant. Considering the system discussed in section 4.2.4 the absorption spectra contains a single peak, with a slight shoulder, see Fig. 4.3. The single peak structure is expected from the isolated dots, see section 5, and the shoulder is due to single particle transitions. The determinant is dominated by single particle transitions around $\hbar\omega$ =0.9 meV (causing the shoulder in the absorption) and in order to identify the collective excitation the region has to be blown up. The magnified region shows the collective excitation around $\hbar\omega$ =1.12 meV. The fact that the zeros of the real and imaginary part do not coincide exactly is due to the adiabatic factor $\hbar\eta$ and the non-zero external field.

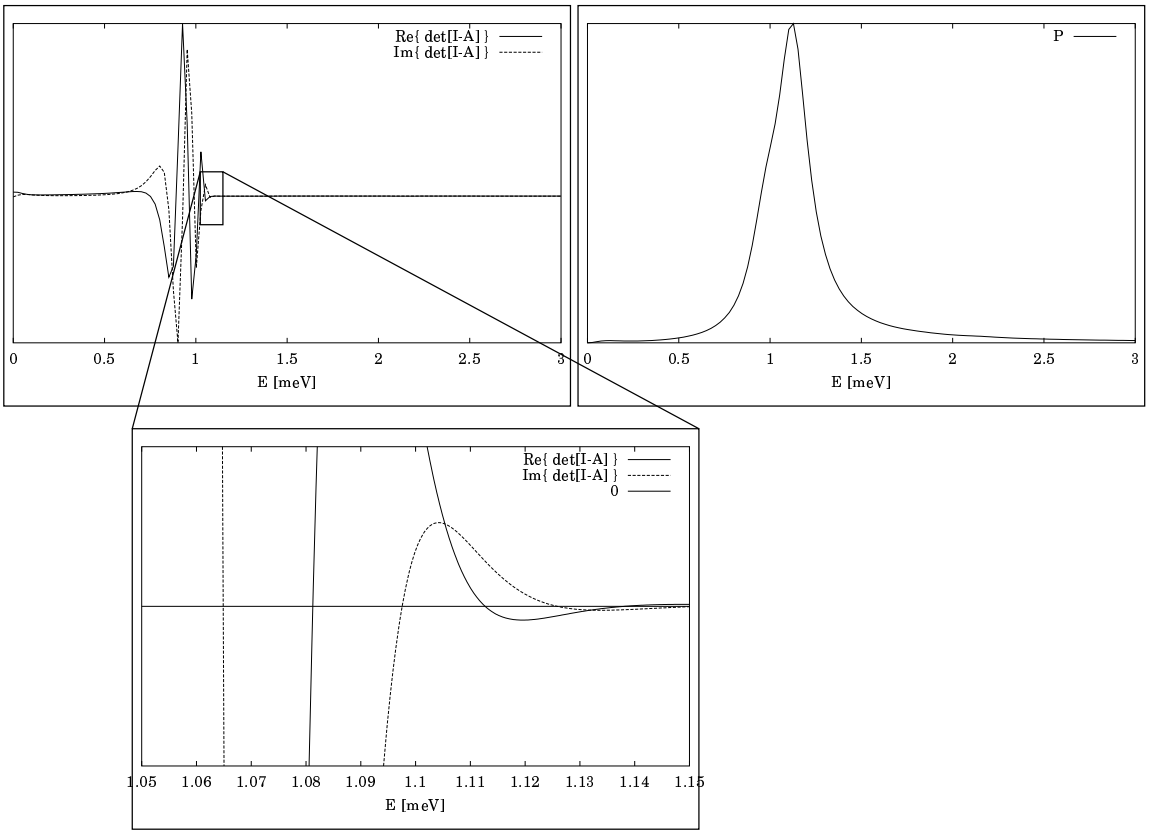

Figure 4.3: The upper left figure shows $\det(\mathsf{I} - \mathsf{A})$ and the lower figure is a magnification of the indicated region. The upper right figure shows the absorption for the same system.

Chapter 5

The FIR absorption of a confined and modulated 2DEG

For parabolic quantum dots the dispersion relation, i.e. the energy of the absorption peak as a function of the magnetic field B, is written as [33, 6]

$$\hbar\omega_{\pm} = \sqrt{(\hbar\omega_0)^2 + \left(\frac{1}{2}\hbar\omega_c\right)^2} \pm \frac{1}{2}\hbar\omega_c\,, \tag{5.1}$$

where ω_c is the cyclotron frequency and ω_0 is the confinement frequency. The confinement of parabolic quantum dots is $V_{\text{conf}} = \frac{1}{2}m^*\omega_0^2(x^2+y^2)$ and thus ω_0 is a characteristic excitation energy of the dot in zero magnetic field. The signs $\pm$ remind us that an external field, circular polarized in one direction (clockwise or counterclockwise), can only excite either of these absorption lines, and in order to excite the other one the polarization has to be reversed [8].

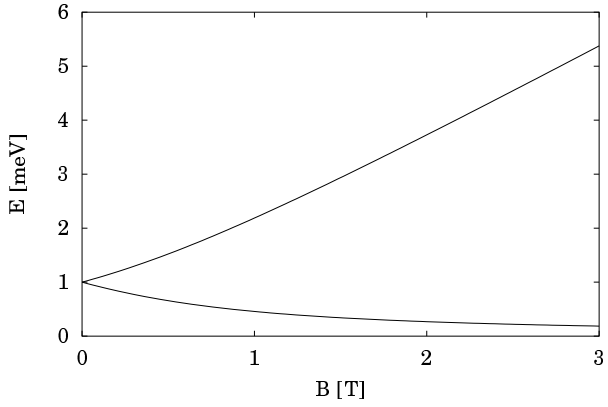

Figure 5.1: The dispersion relation for parabolic dots for a confinement energy $\hbar\omega_0 = 1\,\text{meV}$. For high magnetic field $\omega_c \gg \omega_0$ and the lines go as $\omega_+ \propto B$ and $\omega_- \propto B^{-1}$.

Although this model applies to circularly symmetric parabolic confinement, which is not investigated here, it serves as a valuable tool to understand what kind of absorption one would expect to see in a general confined electron system. Fig. 5.1 shows the two dispersion lines for confinement energy $\hbar\omega_0 = 1\,\mathrm{meV}$. Even though the origin of these absorption lines is complex, their asymptotic behaviour can be understood from a simple classical orbit picture. Consider Fig. 5.2 which shows two different kinds of orbits within a quantum dot of radius R. The orbit at the center of the dot represents orbits where the electrons can move without encountering the dot boundary. The frequency of the motion is $\omega = \omega_c \propto B$. The other orbit represents electrons whose orbits intersect the boundary. Since the electrons are confined to the dot they cannot complete the circular orbit and are reflected at the edges and thus travel around the dot in a skipping orbit [34]. The frequency of this motion can be estimated noting that these electrons feel both the magnetic field and the confinement. The drift velocity is $v_d = \mathcal{E}/B$ where $\mathcal{E}$ is the electric field at the edge of the dot, $\frac{1}{e}\frac{\partial V_{\mathrm{conf}}}{\partial r}|_{r=R}$. The resulting frequency of this motion is $\omega = v_d/R = \omega_0^2/\omega_c \propto B^{-1}$. This simple picture also demonstrates how different polarizations excite these two branches since they essentially move in opposite directions.

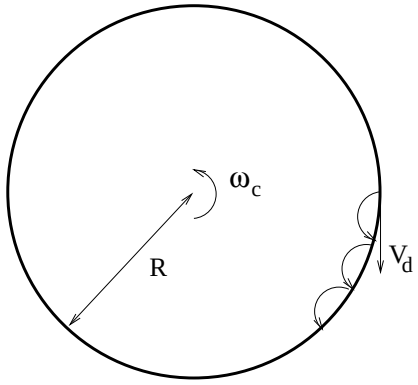

Figure 5.2: A schematic of a quantum dot of radius R. It contains electrons whose motion is unaffected by the edge, orbit at the center of dot. Furthermore electrons close to the edge execute a skipping orbit where they are reflected at the boundary and travel the circumference of the dot in a direction opposite to the cyclotron orbit.

5.1 Changing the size of Σ

Applying a magnetic field to a sample containing electrons (or any charged particle) introduces a length scale in addition to those which previously determined the sample properties. This length is the magnetic length, which is defined as

$$\ell_c = \sqrt{\frac{\hbar}{eB}}. \tag{5.2}$$

In order to consider the competing effects of the hard-wall confinement, i.e. the finite size, and the magnetic field we change the size of the system by increasing the number of unit cells, which are of constant size. In these calculations the size of the unit cell is $50 \times 50\,\mathrm{nm}^2$. The modulation is given by eq. (3.9) where L_x (L_y) is the side length and M_x (M_y) is the number of unit cells in the x (y) direction. The size of the system is thus $M_x \times M_y$ times the size of the unit cell. Keeping the x and y directions equivalent the number of cells in each direction is the same, $M_x = M_y$. The type of modulation is determined by the sign of V_0, and if $V_0 = 0$ the system is homogeneous within Σ.

Before proceeding any further it is necessary to discuss the calculation implementation of eqs. (4.23) and (4.26). These equations are exact, within the present formalism, if the sum includes all possible transitions (the indices α and β denote eigenstates of the system) but only the transitions 'around' the chemical potential are important. The approximation lies in how large we choose this energy interval around the chemical potential. The basic rule of thumbs is that all states up to energy of at least $\mu + \hbar\omega_{\mathrm{Max}}$ should be included. The energy $\hbar\omega_{\mathrm{Max}}$ is the maximum excitation energy of the external field applied to the system. Normally a somewhat larger interval is used to get a correct depolarization shift of the highest energy transitions. A maximum excitation energy of $\hbar\omega_{\mathrm{Max}} = 10\,\mathrm{meV}$ is used in the following calculations.

In these calculations a modulation amplitude of $V_0 = -5$, 0 and $+5\,\mathrm{meV}$ are considered for system sizes corresponding to 1×1, 2×2, 3×3 and 4×4 unit cells. As the system size increases so does the number of states per energy interval. This means that for a fixed ω_{Max} the number of states included in the calculations increases, and increases rather rapidly, and so does the time needed to calculate the absorption. The number of accessible states, i.e. how many states are included in the calculations, is denoted by N_{Pow} and is given in the following table:

$M_x \times M_y$	N_{Pow}
1×1	10
2×2	15
3×3	30
4×4	45

An electron density of one particle per unit cell is used throughout, i.e. $N_s = M_x M_y$, except in the 1×1 case where $N_s = 2$. The temperature is $T = 1\,\mathrm{K}$ and the wavevector is along the diagonal of the system with a wavelength much larger than the system size, i.e. $kL \ll 1$.

5.2 Results of the calculations

The absorption spectrum for the 1×1 system with modulation amplitude $V_0 = 0\,\mathrm{meV}$ is shown in Fig. 5.3. The spectrum is dominated by two lines that converge as the magnetic field goes to zero. Similar behaviour is well known for a single quantum dot with parabolic confinement [7, 8]. The panel to the right shows the position of

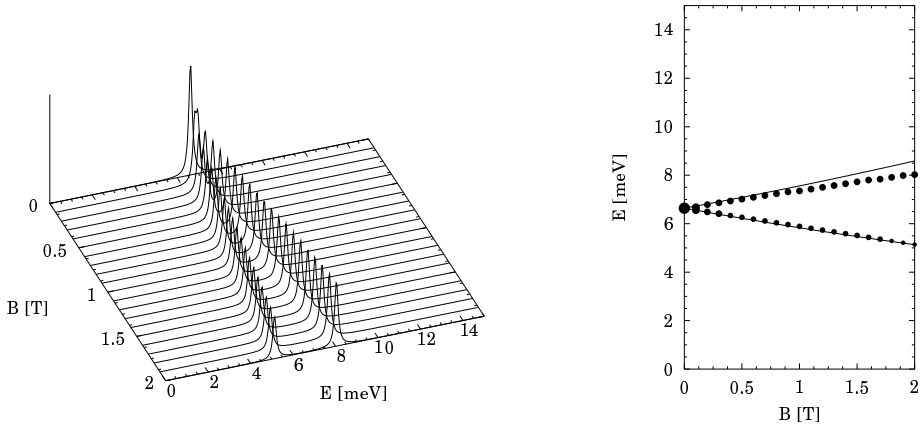

Figure 5.3: The power absorption as a function of energy E and B, to the left, and the dispersion graph for the 1×1 system, $V_0 = 0\,\text{meV}$.

the absorption peaks as a function of the magnetic field, so-called dispersion graph. The symbol size indicates the oscillator strength at each point. The solid lines show the dispersion relations of a parabolic quantum dot, see eq. (5.1), where the confining energy $\hbar\omega_0$ is assumed to coincide with the energy of the peak with highest oscillator strength at $B = 0\,\text{T}$.

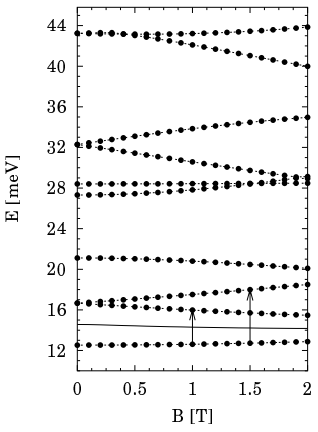

Figure 5.4: The energy spectrum as a function of magnetic field B for the 1×1 system for modulation amplitude $V_0 = 0\,\text{meV}$. The solid line shows the chemical potential. The arrows show the 1→2 and 1→3 transitions.

The lower branch follows ω_- very well but the upper branch starts to deviate from ω_+ as the magnetic field increases. The deviation is due to anti-crossing caused by the square geometry, which induces quadrupole contribution in the absorption. This behaviour is seen in both measurements and calculations [8, 10]. It can be understood from the Darwin-Fock energy diagram in Fig. 5.4. The solid line denotes the chemical

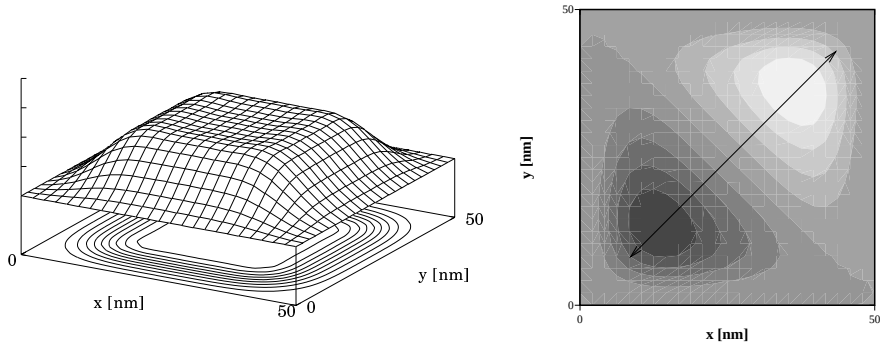

Figure 5.5: The ground state density, to the left, and a contour plot of the induced density for the 1×1 system for $V_0 = 0\,\text{meV}$ modulation at $B = 0\,\text{T}$ and $E = 6.64\,\text{meV}$. The arrow indicates the 50 nm length-scale.

potential. The square geometry splits states 4,5 and 6, which are degenerate in circular symmetry [5], causing state 4 to be lowered in energy (to clarify this discussion the arrows in Fig. 5.4 show the 1→2 and 1→3 transitions). As states 3 and 4 get closer, with increasing magnetic field, their interaction gets stronger causing the 1→3 transition branch to be pushed down from ω_+.

It is possible to interprete the absorption spectrum in terms of the ground state here because the levels are few. As the levels get more dense, as happens for larger systems, the depolarization shift makes this comparison very difficult. Because the lowest states remain relatively unchanged except for an energy shift when the modulation is changed, the absorption spectra remains almost identical for different modulations.

Parabolic, circularly confined dots are circularly symmetric. The electron density of the square dot, with no modulation potential $V_0 = 0\,\text{meV}$, is shown in the panel to the left in Fig. 5.5. Its structure has clear signs of the square confinement, i.e. the contour lines are squares with rounded corners.

The induced density has a strong dipole motion, along the diagonal, about the center which is evident in the contour plot in the panel to the right. The motion bears strong resemblance with the center-of-mass motion which is characteristic of quantum dots [2, 5]. The boundary limits the charge motion thus forming the triangular shape of the contours.

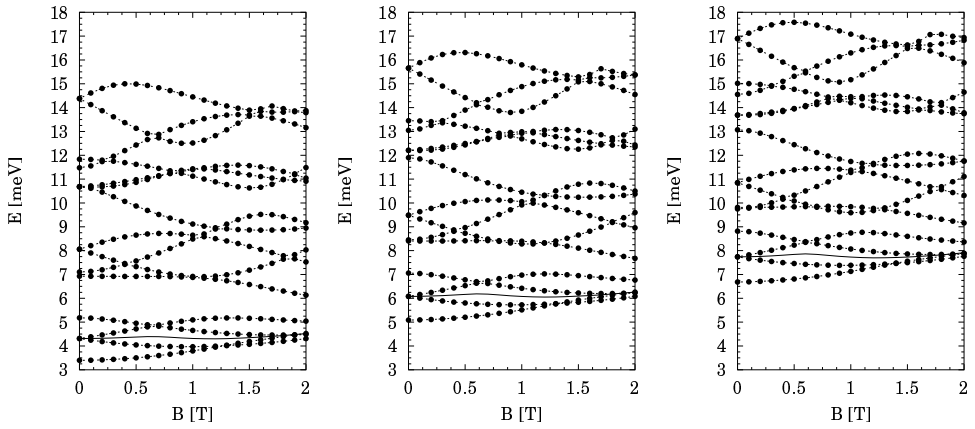

Figure 5.6: The energy spectrum as a function of magnetic field B for the 2×2 system for modulation amplitudes, from left to right, $V_0 = -5$, 0 and $+5$ meV. The solid line shows the chemical potential.

By increasing the side lengths the energy levels become more dense. For the 2×2 system the screened potential amplitude is comparable to the level spacing and modulation effects are seen in the absorption spectra in Fig. 5.8. From top to bottom the modulation amplitudes are $V_0 = -5$, 0 and $+5$ meV. For all modulations the square

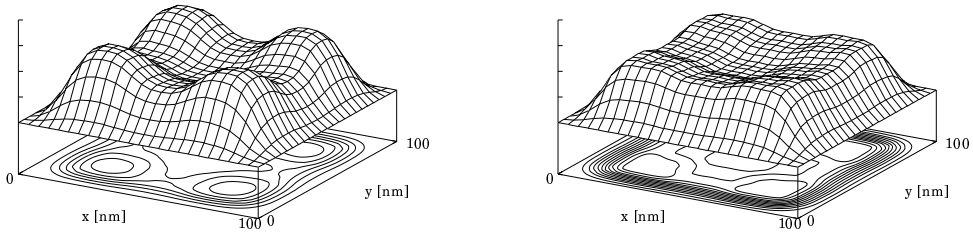

Figure 5.7: The densities for modulation amplitudes $V_0 = -5$ meV, to the left, and $V_0 = 0$ meV for the 2×2 system.

splitting is seen as an anti-crossing around the ω_+ mode. It is interesting how the spectrum approaches a more 'clean' square dot spectrum as the modulation amplitude is changed from $V_0 = -5$ meV to $+5$ meV. The top panel in Fig. 5.8 shows a substantial gap between the absorption branches at $B = 0$ T which can be understood from the Darwin-Fock diagram in Fig. 5.6. The first four states are lowered in energy for the $V_0 = -5$ meV modulation, corresponding to four states localized around each of the potential minima. This lowering happens to coincide with the square splitting so the

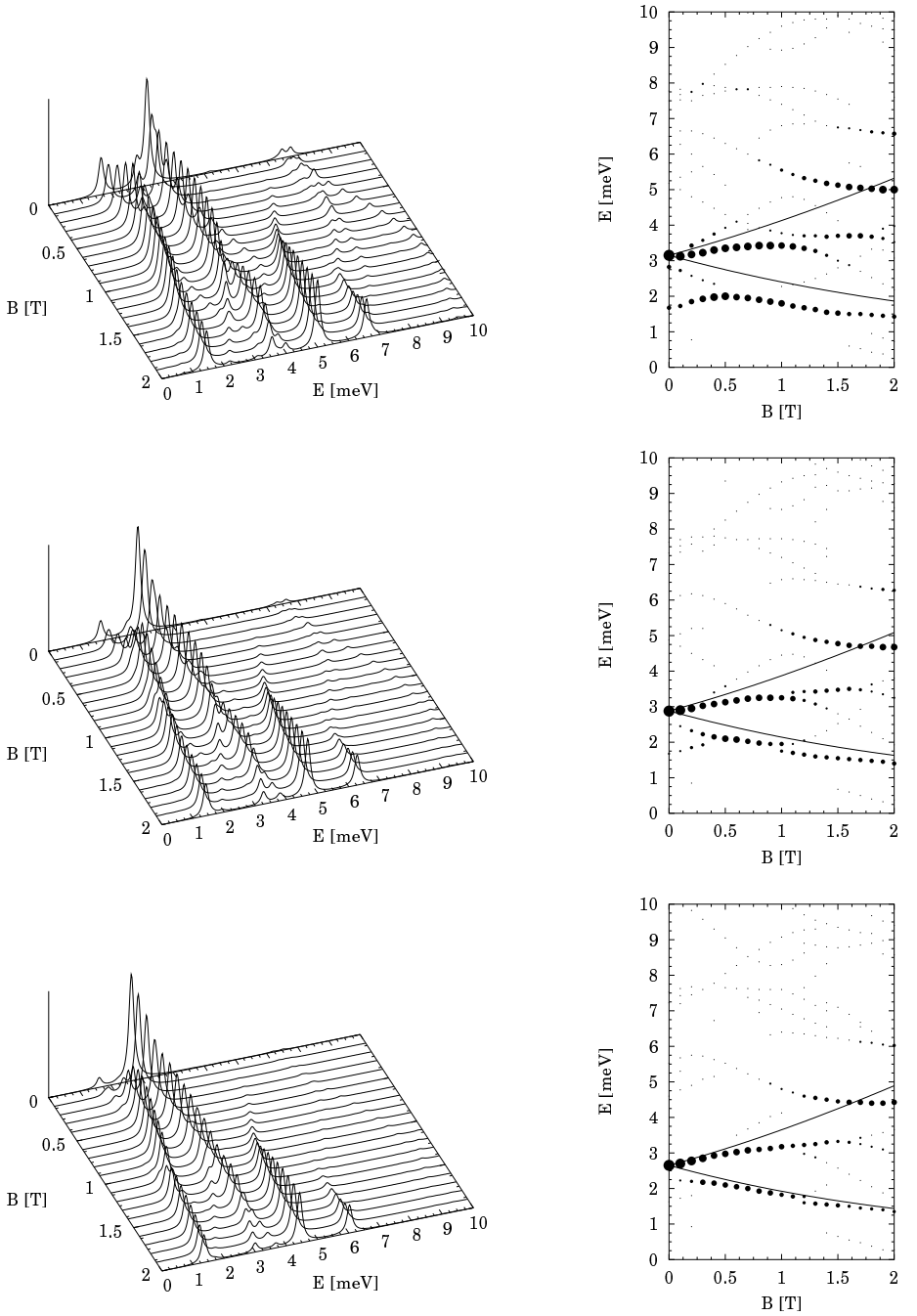

Figure 5.8: The power absorption as a function of energy E and B, left, and the dispersion graph for a 2×2 system for modulation amplitudes, from top to bottom, $V_0 = -5$, 0 and $+5$ meV.

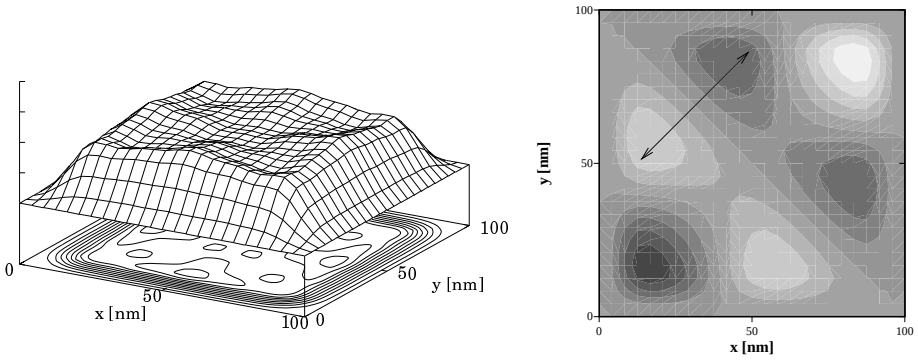

Figure 5.9: The ground state density, to the left, and a contour plot of the induced density for the 2×2 system for $V_0 = +5\,\mathrm{meV}$ modulation at $B = 0\,\mathrm{T}$ and $E = 2.65\,\mathrm{meV}$. The arrow indicates the 50 nm length-scale.

gap due to the geometry is enhanced. The $V_0 = +5\,\mathrm{meV}$ modulation tends to close this gap, see bottom panel in Fig. 5.8.

The electron density, for zero modulation, has a four peak structure, the panel to the right in Fig. 5.7. The electron repulsion causes the lowest energy configuration to be one electron in each corner. Adding a $V_0 = -5\,\mathrm{meV}$ modulation amplifies this structure, panel to the left, since the potential minima coincides with the Hartree potential minima. The lowest branch in the top panel in Fig. 5.8 resembles the ω_- branch of an antidot [4, 35]. In the case of the $V_0 = -5\,\mathrm{meV}$ modulation the density has similar features as a single antidot, i.e. the density is lowered in the center of the system.

The density for the $V_0 = +5\,\mathrm{meV}$ modulation has a different structure since the modulation maxima coincides with the Hartree potential minima. This smooths out the density, giving a more single dot-like look, as is seen in the panel to the left in Fig. 5.9. The induced density shows a dipole motion along the diagonal but there is an added modulation with wavelength of about 50 nm, as indicated by the arrow in the panel to the right.

The absorption spectra of the 3×3 system in Fig. 5.12 show the reduction of the square splitting, i.e. the absence of strong branches above the upper one. The upper branch is composed of many branches which all gain oscillator strength around the region of the parabolic dot dispersion curve. Again the spectra show an evolution from a more complex absorption for $V_0 = -5\,\mathrm{meV}$ modulation to a single dot-like behaviour for $V_0 = +5\,\mathrm{meV}$ modulation. The gap in the absorption spectra at $B = 0\,\mathrm{T}$ seen in

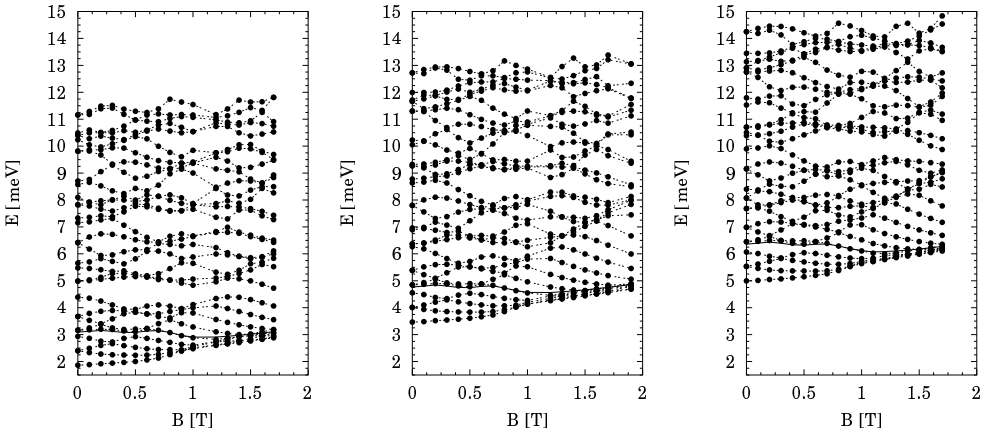

Figure 5.10: The energy spectrum as a function of magnetic field B for the 3×3 system for modulation amplitudes, from left to right, $V_0 = -5$, 0 and $+5\,\mathrm{meV}$. The solid line shows the chemical potential.

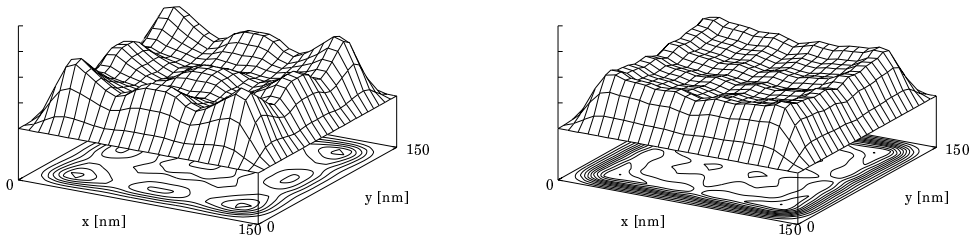

Figure 5.11: The densities for modulation amplitudes $V_0 = -5\,\mathrm{meV}$, to the left, and $V_0 = 0\,\mathrm{meV}$ for the 3×3 system.

the top panel can be understood, as before, because nine states get lowered in energy corresponding to the 3×3 minima in the potential. The leftmost panel in Fig. 5.10 shows a gap at $E \approx 4.7\,\mathrm{meV}$ for $B = 0\,\mathrm{T}$ with 9 states below it. Due to the increased

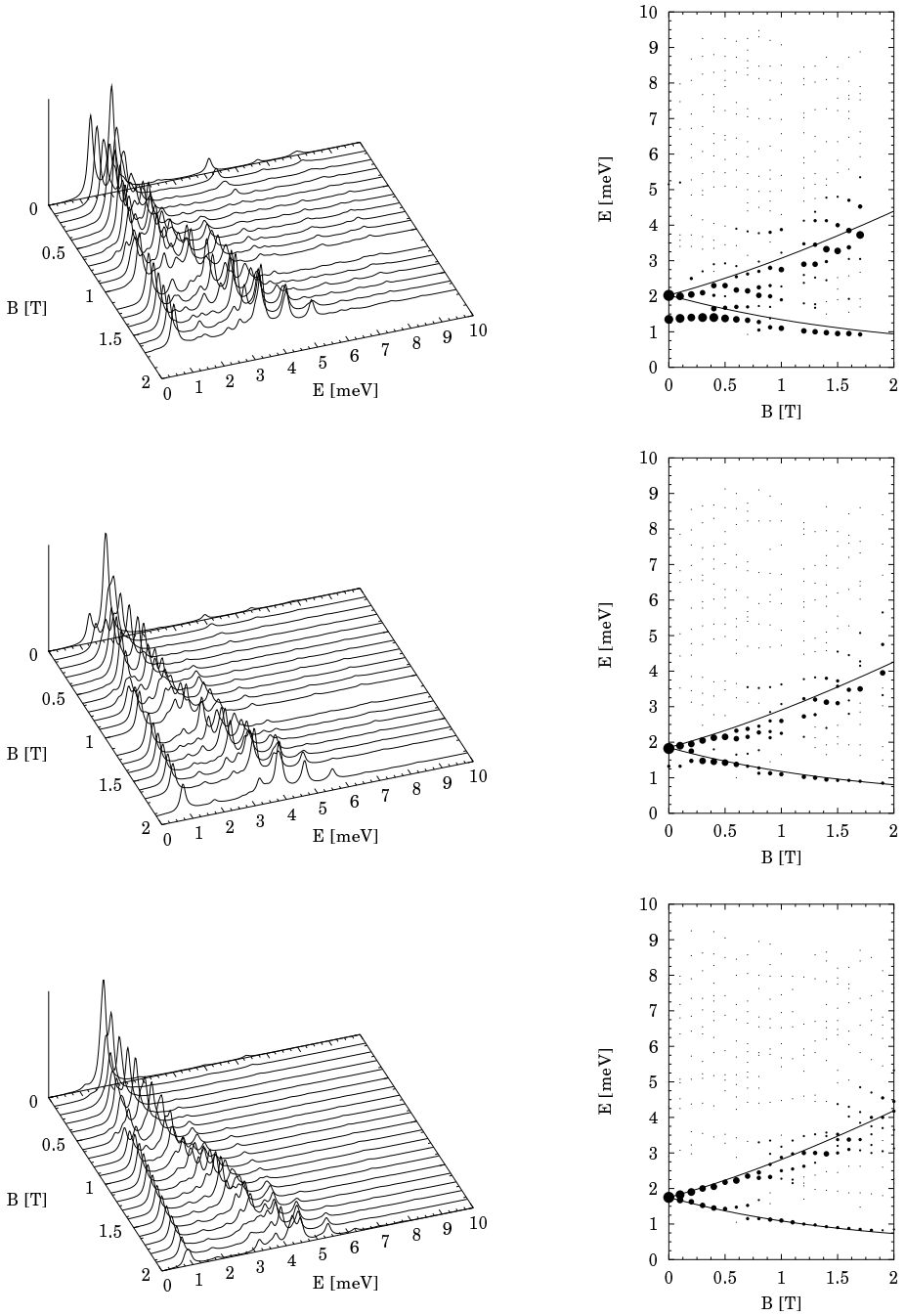

Figure 5.12: The power absorption as a function of energy E and B, left, and the dispersion graph for a 3×3 system for modulation amplitudes, from top to bottom, $V_0 = -5$, 0 and $+5$ meV.

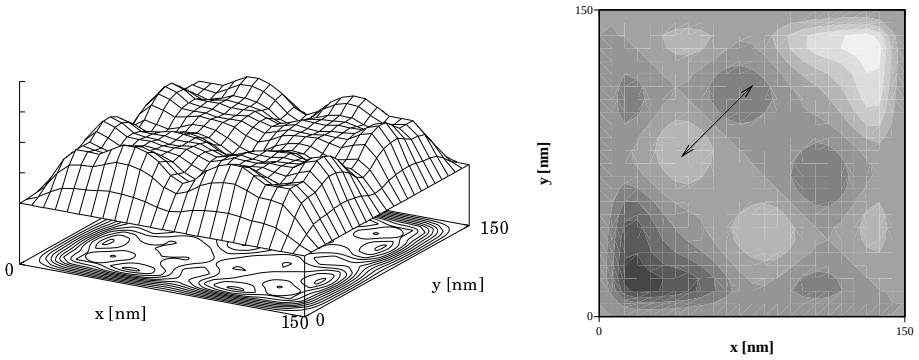

Figure 5.13: The ground state density, to the left, and a contour plot of the induced density for the 3×3 system for $V_0 = +5\,\mathrm{meV}$ modulation at $B = 0\,\mathrm{T}$ and $E = 1.75\,\mathrm{meV}$. The arrow indicates the 50 nm length-scale.

size the states are more dense than in Figs. 5.4 and 5.6 and the square splitting is not as noticeable.

For $V_0 = 0\,\mathrm{meV}$ the electron density is highest close to the edge because the Hartree potential is lowest there, see the panel to the left in Fig. 5.11. This behaviour is easy to understand in terms of electron-electron repulsion, i.e. by arranging themselves near the boundary they can minimize the repulsion force. The $V_0 = -5\,\mathrm{meV}$ modulation causes bumps in this structure around the potential minima. The induced density in Fig. 5.13, for $V_0 = +5\,\mathrm{meV}$, still shows a strong dipole motion plus a charge motion with wavelength comparable to the modulation wavelength.

The Darwin-Fock diagram for the 4×4 system with $V_0 = -5\,\text{meV}$ modulation in the panel to the left in Fig. 5.14 shows a gap above the first 16 states being lowered by the potential. The size of the gap and the effects of the square confinement are reduced due to the increased energy level density. The $V_0 = +5\,\text{meV}$ modulation closes the gap and a new feature, not seen in the other systems, is the formation of Landau levels for high magnetic fields. The panel to the right in Fig. 5.14 shows how the energy levels condense at $E \approx 5.6\,\text{meV}$ and $E \approx 8.7\,\text{meV}$ for $B = 1.8\,\text{T}$, which is in agreement with the Landau level separation of $\Delta E = 3.1\,\text{meV}$ for this magnetic field. The same applies to the left panel where the first two Landau bands are situated at $E \approx 2.3\,\text{meV}$ and $E \approx 5.2\,\text{meV}$ for $B = 1.7\,\text{T}$, again in agreement with a Landau level separation of $\Delta E = 2.9\,\text{meV}$. The Landau bands correspond to bulk states and in between them are

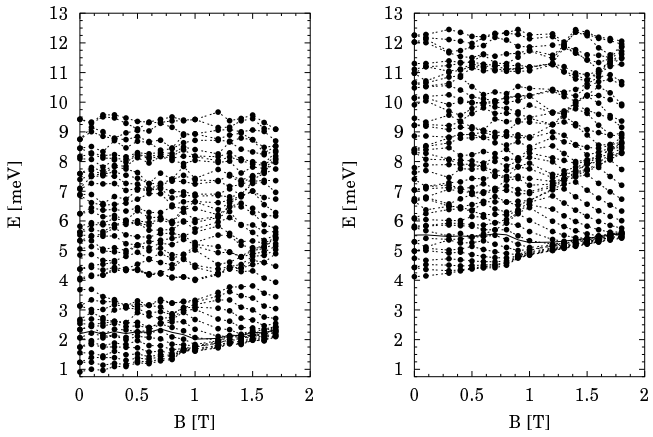

Figure 5.14: The energy spectrum as a function of magnetic field B for the 4×4 system for modulation amplitudes $V_0 = -5\,\text{meV}$, to the left, and $V_0 = +5\,\text{meV}$. The solid line shows the chemical potential.

edge states which get more sparse as the magnetic field, or system size increases. Note that the chemical potential lies in the first Landau band.

The absorption branches for the $V_0 = -5\,\text{meV}$ modulation in the upper panel in Fig. 5.15 converge at $B = 0\,\text{T}$, and although the branches are somewhat scattered their oscillator strength is greatest around $\omega_{\pm}$. In the case of the $V_0 = +5\,\text{meV}$ modulation, seen in the lower panel, the absorption shows a still stronger tendency towards the parabolic dot dispersion. The effects of the modulation on the induced density are evident in the panel to the right in Fig. 5.16. The electron density has a definite fingerprint from the modulation, i.e. density minimas around the potential maximas and in between them the density has maximas.

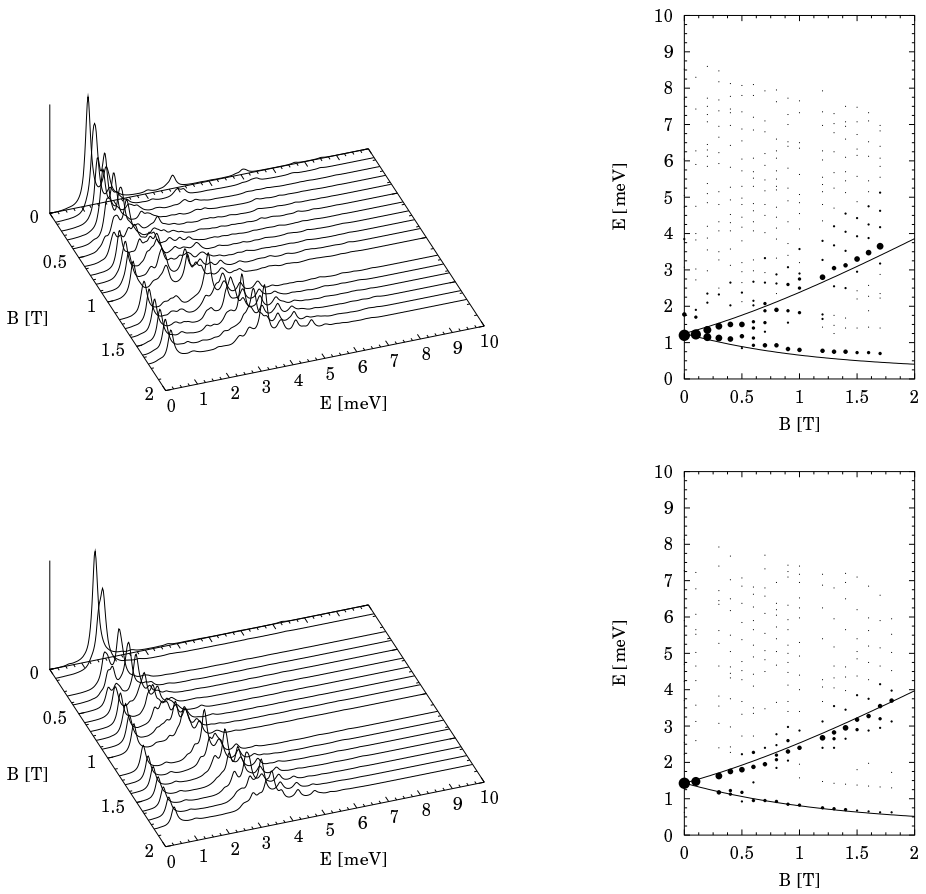

Figure 5.15: The power absorption as a function of energy E and B, to the left, and the dispersion graph for the 4×4 system for modulation amplitudes $V_0 = -5$, upper panel, and $V_0 = +5$ meV.

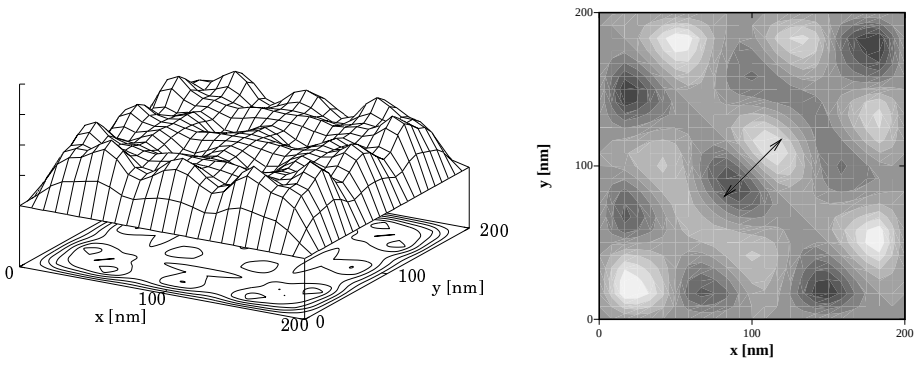

Figure 5.16: The ground state density, to the left, and a contour plot of the induced density for the 4×4 system for $V_0 = +5$ meV modulation at $B = 0$ T and $E = 1.43$ meV. The arrow indicates the 50 nm length-scale.

Chapter 6

Summary and discussion

When the dispersion graphs for the $V_0 = +5\,\mathrm{meV}$ modulation are compared for all the system sizes some interesting features emerge, as seen in Fig. 6.1. One of the most striking is how the spectrum evolves from the simple two branch structure in the 1×1 system to the 4×4 one which again shows, in general, the same behaviour. It is important to stress that although the absorption may be similar the ground states are totally different and the origin of the two-branch behaviour is not the same in both cases.

In order to clarify this evolution of the spectra it is instructive to first consider the opposite ends, i.e. the 1×1 and 4×4 systems. The 1×1 system is strongly confined and the energy level separation is large. Since there are only two electrons in the system the absorption is dominated by the 1→2 and the 1→3 transition. The magnetic field lifts the degeneracy of levels 2 and 3, see Fig. 5.4, and this splitting is the origin of the two branch structure in the absorption.

The 4×4 system has a dense energy spectrum where the levels condense into Landau bands at high magnetic fields. In order to explain the absorption in this case a very different approach has to be used. As is seen in the Darwin-Fock diagram, see the panel to the right in Fig. 5.14, Landau bands are formed and this indicates that the the electrons 'see' a nearly infinite system. The finite width of the bands is due to the modulation and the states in between the bands are edge states. Both these factors contribute to making the two branch structure deviate slightly from the dispersion relation in eq. (5.1).

The intermediate cases, especially the 2×2 system, indicate that there is an transition region from the strong confinement to the large system. In this region many processes are competing, i.e. the finite size, the modulation and the magnetic field. This is represented in the dispersion graph which is more complex than in the other cases. Describing this behaviour on a microscopic level is not possible so this region will not be discussed further here.

When the the 4×4 system is considered as a candidate for an infinite system one is

tempted to apply, or at least discuss, Kohn's theorem [36]. This theorem[1] states that an infinite, homogeneous system in magnetic field can only be excited at a frequency $\omega = \omega_c$. The theorem can be used to explain the absorption in the 4×4 for high magnetic fields. The lower branch ω_- is due to the edge states, as was discussed in chapter 5. The system is not homogenous but there are many states, i.e. the states which constitute the Landau bands, which do not experience the boundary of the system. These states form the backbone of the ω_+-like absorption branch and encourage the application of the theorem.

An experimental implementation of these calculations should be possible now or, at least, in the near future. Making the modulation potential with wavelength of only 50 nm may be difficult but it should be relatively easy to fabricate the zero modulation, finite systems. To boost the signal-to-noise ratio of the transmission measurements (experiments measure transmission, not absorption) an array of finite systems should be made such that the distance between adjacent systems would be much larger than the modulation amplitude or individual subsystem size.

[1]Named after Walter Kohn who received the Nobel price in chemistry in 1998

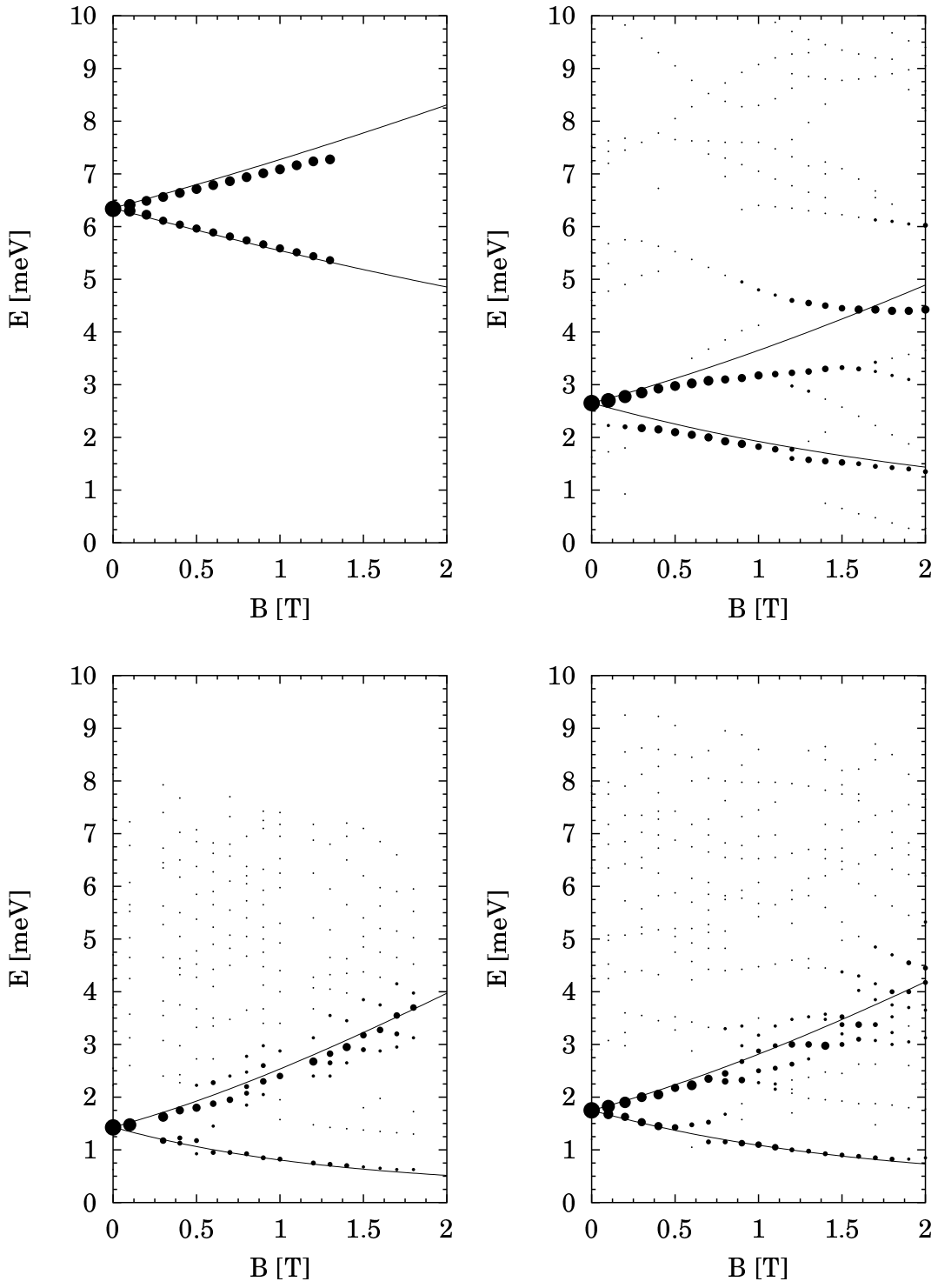

Figure 6.1: The dispersion graphs for $V_0 = +5\,\text{meV}$, clockwise from the upper left corner, for the 1×1, 2×2, 3×3 and 4×4 systems.

Chapter 7

Acknowledgements

I would like to thank professor Viðar Guðmundsson for being a very good and patient supervisor and giving me the opportunity to work in this field. Also I would like to thank Andrei Manolescu for helping me to understand physics better, especially the many-body theory. Special thanks go to professor Poul Erik Lindelof who taught the course Mesoscopic Physics at the University of Copenhagen where I learned how nanoscale samples are fabricated and measured.

I also want to mention my gymnasium mathematics teacher dr. Áskell Harðarson who initially inspired me to study physics.

This work was supported by the Student Research Fund, the Icelandic Natural Science Foundation, the University of Iceland Research Fund and the NorFA Network on Mesoscopic Physis.

Appendix A

Matrix elements

The matrix elements in eq. (3.16) are defined as

$$\begin{aligned} \mathsf{H}_{m_1n_1,m_2n_2} &= (\chi_{m_1n_1}, H\chi_{m_2n_2}) \\ &= (\chi_{m_1n_1}, T_{\|}\chi_{m_2n_2}) + (\chi_{m_1n_1}, V_{\rm mod}\chi_{m_2n_2}) \\ &= \mathsf{T}_{m_1n_1,m_2n_2} + \mathsf{V}_{m_1n_1,m_2n_2}. \end{aligned} \tag{A.1}$$

Using the kinetic operator in eq. (3.8) one can write the T matrix elements as

$$\begin{aligned} \mathsf{T}_{m_1n_1,m_2n_2} &= \frac{1}{2}\hbar\omega_c \Bigg\{ \left(\chi_{m_1n_1}, -\ell_c^2\left[\frac{\partial^2}{\partial x^2} + \frac{\partial^2}{\partial x^2}\right]\chi_{m_2n_2}\right) \\ &\quad + \left(\chi_{m_1n_1}, i\left[\left(y - \frac{L_y}{2}\right)\frac{\partial}{\partial x} - \left(x - \frac{L_x}{2}\right)\frac{\partial}{\partial y}\right]\chi_{m_2n_2}\right) \\ &\quad + \left(\chi_{m_1n_1}, \frac{1}{4\ell_c^2}\left[\left(x - \frac{L_x}{2}\right)^2 + \left(y - \frac{L_y}{2}\right)^2\right]\chi_{m_2n_2}\right)\Bigg\} \\ &= \frac{1}{2}\hbar\omega_c \Bigg\{ (2\pi)^2\left[m_2^2\left(\frac{L_x}{2\ell_c}\right)^2 + n_2^2\left(\frac{L_y}{2\ell_c}\right)^2\right]\delta_{m_1m_2}\delta_{n_1n_2} \\ &\quad + i\left[\left(\frac{L_x}{L_y}\right)^{-1} I_1(m_1,m_2)I_2(n_1,n_2) - \left(\frac{L_x}{L_y}\right) I_2(m_1,m_2)I_1(n_1,n_2)\right] \\ &\quad + \left[\left(\frac{L_x}{2\ell_c}\right)^2 I_3(m_1,m_2)\delta_{n_1n_2} + \left(\frac{L_y}{2\ell_c}\right)^2 \delta_{m_1m_2}I_3(n_1,n_2)\right]\Bigg\}, \end{aligned} \tag{A.2}$$

where the integrals I_1, I_2 and I_3 are defined as

$$\begin{aligned} I_1(m_1,m_2) &= 2\int_0^1 du \sin(m_1\pi u)\frac{\partial}{\partial u}\sin(m_2\pi u) \\ &= \begin{cases} \frac{2m_1m_2}{(m_1^2-m_2^2)}(1-(-1)^{m_1+m_2}) & m_1 \neq m_2 \\ 0 & \text{otherwise} \end{cases} \end{aligned}$$

$$
\begin{aligned}
I_2(m_1,m_2) &= 2\int_0^1 du \sin(m_1\pi u)\left(u-\frac{1}{2}\right)\sin(m_2\pi u) \\
&= \begin{cases} -\frac{4m_1m_2}{(m_1^2-m_2^2)^2}(1-(-1)^{m_1+m_2}) & m_1 \neq m_2 \\ 0 & \text{otherwise} \end{cases}
\end{aligned}
$$

$$
\begin{aligned}
I_3(m_1,m_2) &= 2\int_0^1 du \sin(m_1\pi u)\left(u-\frac{1}{2}\right)^2\sin(m_2\pi u) \\
&= \begin{cases} \frac{4m_1m_2}{(m_1^2-m_2^2)^2}(1+(-1)^{m_1+m_2}) & m_1 \neq m_2 \\ \frac{1}{2}\left(1-\frac{1}{\pi^2 m_2^2}\right) & \text{otherwise} \end{cases}
\end{aligned}
$$

The factors $(1 \pm (-1)^{m_1+m_2})$ rarify the matrix, making the calculations less time consuming. This is a result of the gauge in eq. (3.5) being a odd function about the center of the system.

The potential matrix elements are defined as

$$
\begin{aligned}
\mathsf{V}_{m_1n_1,m_2n_2} &= (\chi_{m_1n_1}, V_{\text{mod}}\chi_{m_2n_2}) \\
&= V_0\left[\frac{1}{2}\delta_{m_1m_2}-\frac{1}{2}I_4(m_1,m_2)\right]\left[\frac{1}{2}\delta_{n_1n_2}-\frac{1}{2}I_4(n_1,n_2)\right], \qquad \text{(A.3)}
\end{aligned}
$$

where the integral I_4 is defined as

$$
\begin{aligned}
I_4(m_1,m_2) &= 2\int_0^1 du \sin(m_1\pi u)\cos(2M\pi u)\sin(m_2\pi u) \\
&= \begin{cases} \frac{1}{2} & |m_1-m_2| = 2M \\ -\frac{1}{2} & m_1+m_2 = 2M \\ 0 & \text{otherwise} \end{cases}
\end{aligned}
$$

Appendix B

The $\sigma - \epsilon$ relationship

By using the continuity equation, Poisson's equation and generalized Ohm's law we can relate the conductivity tensor $\hat{\sigma}$ and the dielectric function ϵ. The generalized Ohm's law [23] plays the role of a constitutive equation connecting the current density $\mathbf{J}$ to the total electric field $\mathbf{E}$

$$\mathbf{J}(\mathbf{r}) = \int d^3\mathbf{r}' \hat{\sigma}(\mathbf{r}, \mathbf{r}') \mathbf{E}(\mathbf{r}'). \tag{B.1}$$

Other forms of constitutive equations may be used [23]. The Fourier transform of the current density is written as

$$\begin{aligned}
\mathbf{J}(\mathbf{k}) &= \int d^3\mathbf{r}'' \mathbf{J}(\mathbf{r}'') e^{-i\mathbf{k}\cdot\mathbf{r}''} \\
&= \int d^3\mathbf{r}'' d^3\mathbf{r}' \hat{\sigma}(\mathbf{r}'', \mathbf{r}') \frac{1}{(2\pi)^3} \int d^3\mathbf{q} \mathbf{E}(\mathbf{q}) e^{i\mathbf{q}\cdot\mathbf{r}'} e^{-i\mathbf{k}\cdot\mathbf{r}''} \\
&= \frac{1}{2\pi} \int dq_z d^2\mathbf{q}_\parallel \left\{ \frac{1}{(2\pi)^2} \int d^3\mathbf{r}'' d^3\mathbf{r}' \hat{\sigma}(\mathbf{r}'', \mathbf{r}') e^{i\mathbf{q}\cdot\mathbf{r}'} e^{-i\mathbf{k}\cdot\mathbf{r}''} \right\} \mathbf{E}(\mathbf{q}) \\
&= \frac{1}{2\pi} \int dq_z d^2\mathbf{q}_\parallel \hat{\sigma}(\mathbf{k}, \mathbf{q}) (-i\mathbf{q}) \phi_{\rm sc}(\mathbf{q}_\parallel, q_z),
\end{aligned}$$

where $\mathbf{E}(\mathbf{q}) = (-i\mathbf{q})\phi_{\rm sc}(\mathbf{q})$ and $\hat{\sigma}(\mathbf{k}, \mathbf{q})$ is the Fourier transform of the conductivity tensor. For 2DEGs the tensor can be written as a 2×2 matrix which only depends on the lateral variables

$$\hat{\sigma}(\mathbf{k}, \mathbf{q}) = \hat{\sigma}(\mathbf{k}_\parallel, \mathbf{q}_\parallel), \tag{B.2}$$

where $\parallel$ subscript denotes the lateral subspace. The current density is thus

$$\mathbf{J}(\mathbf{k}) = \int d^2\mathbf{q}_\parallel \hat{\sigma}(\mathbf{k}_\parallel, \mathbf{q}_\parallel)(-i\mathbf{q}_\parallel) \frac{1}{2\pi} \int dq_z \phi_{\rm sc}(\mathbf{q}_\parallel, q_z). \tag{B.3}$$

The Fourier transform of the continuity equation is [37]

$$-i\omega\rho_{\rm ind}(\mathbf{k}, \omega) + i\mathbf{k}\cdot\mathbf{J}(\mathbf{k}) = 0.$$

Inserting eq. (B.3) into this equation and solving for the density one can write it as

$$\rho_{\rm ind}(\mathbf{k},\omega) = \frac{-i}{\omega}\int d^2\mathbf{q}_\parallel \mathbf{k}_\parallel \cdot \hat{\sigma}(\mathbf{k}_\parallel,\mathbf{q}_\parallel)\mathbf{q}_\parallel \frac{1}{2\pi}\int dq_z \phi_{\rm sc}(\mathbf{q}_\parallel,q_z). \tag{B.4}$$

The Poisson equation, in CGS units, in the Fourier space is written as

$$k^2\phi_{\rm ind}(\mathbf{k}) = 4\pi\rho_{\rm ind}(\mathbf{k}).$$

This equation relates the induced field $\phi_{\rm ind}$ to the total field $\phi_{\rm sc}$ through eq. (B.4). Performing the inverse Fourier transform in the q_z variable one gets

$$\begin{aligned}
\phi_{\rm ind}(\mathbf{k}_\parallel,z) &= \frac{1}{2\pi}\int dk_z \phi_{\rm ind}(\mathbf{k}_\parallel,k_z)e^{ik_z z} \\
&= \frac{1}{2\pi}\int dk_z \frac{4\pi\rho_{\rm ind}(\mathbf{k})}{k^2}e^{ik_z z} \\
&= 4\pi\rho_{\rm ind}(\mathbf{k}_\parallel)\frac{1}{2\pi}\int dk_z \frac{e^{-ik_z z}}{k_\parallel^2+k_z^2} \\
&= -\frac{2\pi i}{k_\parallel\omega}\int d^2\mathbf{q}_\parallel \mathbf{k}_\parallel\cdot\hat{\sigma}(\mathbf{k}_\parallel,\mathbf{q}_\parallel)\mathbf{q}_\parallel\frac{1}{2\pi}\int dq_z\phi_{\rm sc}(\mathbf{q}_\parallel,q_z)e^{-k_\parallel|z|}.
\end{aligned}$$

Since we are interested in the 2DEG, i.e. $z=0$, this equation becomes

$$\phi_{\rm ind}(\mathbf{k}_\parallel,0) = -\frac{2\pi i}{k_\parallel\omega}\int d^2\mathbf{q}_\parallel\mathbf{k}_\parallel\cdot\hat{\sigma}(\mathbf{k}_\parallel,\mathbf{q}_\parallel)\mathbf{q}_\parallel\phi_{\rm sc}(\mathbf{q}_\parallel,0), \tag{B.5}$$

where the integral over q_z was interpreted as the inverse Fourier transform for $z=0$. The principle of superposition relates the external, induced and total field

$$\phi_{\rm sc} = \phi_{\rm ext} + \phi_{\rm ind}$$

and using eq. (4.35) one can write this equation as

$$\begin{aligned}
\phi_{\rm ext}(\mathbf{k}_\parallel,0) &= \phi_{\rm sc}(\mathbf{k}_\parallel,0) - \phi_{\rm ind}(\mathbf{k}_\parallel,0) \\
&= \int d^2\mathbf{q}_\parallel\left\{\delta(\mathbf{k}_\parallel-\mathbf{q}_\parallel)+\frac{2\pi i}{k_\parallel\omega}\mathbf{k}_\parallel\cdot\hat{\sigma}(\mathbf{k}_\parallel,\mathbf{q}_\parallel)\mathbf{q}_\parallel\right\}\phi_{\rm sc}(\mathbf{q}_\parallel,0) \\
&\equiv \int d^2\mathbf{q}_\parallel\epsilon(\mathbf{k}_\parallel,\mathbf{q}_\parallel)\phi_{\rm sc}(\mathbf{q}_\parallel,0)
\end{aligned}$$

yielding the relation

$$\epsilon(\mathbf{k}_\parallel,\mathbf{q}_\parallel) = \delta(\mathbf{k}_\parallel-\mathbf{q}_\parallel)+\frac{2\pi i}{k_\parallel\omega}\mathbf{k}_\parallel\cdot\hat{\sigma}(\mathbf{k}_\parallel,\mathbf{q}_\parallel)\mathbf{q}_\parallel. \tag{B.6}$$

Note that this equation was derived using fundamental relations, except for the constitutive equation. The constant field, 3D version of this equation is the familiar equation [30]

$$\epsilon = 1+\frac{4\pi i}{\omega}\sigma. \tag{B.7}$$

Bibliography

[1] V. Gudmundsson, I. Magnusdottir, and S. I. Erlingsson, Physica E **1**, 235 (1997).

[2] V. Gudmundsson, Phys. Rev. B **57**, 3989 (1998).

[3] A. Manolesco and V. Gudmundsson, Phys. Rev. B **57**, 1668 (1998).

[4] S. A. Mikhailov, Phys. Rev. B **54**, 10335 (1996).

[5] P. A. Maksym and T. Chakraborty, Phys. Rev. Lett **65**, 108 (1990).

[6] D. A. Broido, K. Kempa, and P. Bakshi, Phys. Rev. B **42**, 11400 (1990).

[7] D. Pfannkuche, V. Gudmundsson, P. Hawrylak, and R. Gerhardts, Solid-State Electronics **37**, 1221 (1994).

[8] V. Gudmundsson *et al.*, Phys. Rev. B **51**, 17744 (1995).

[9] A. Brataas, V. Gudmundsson, A. G. Mal'shukov, and K. A. Chao, J. Phys.: Condens. Matter **8**, 4797 (1996).

[10] R. Ugajin, Phys. Rev. B **53**, 6963 (1996).

[11] C. W. J. Beenakker and H. van Houten, in *Quantum Transport in Semiconductor Nanostructures*, Vol. 44 of *Sol. State Phys.*, edited by H. Ehrenreich and D. Turnbull (Academic Press, New York, 1991).

[12] U. Rössler, in *Quantum Transport in Ultrasmall Devices*, edited by D. Ferry, H. L. Grubin, C. Jacoboni, and A. Jauho (Plenum Press, New York, 1995), pp. 77–110.

[13] H. L. Störmer *et al.*, Solid State Communications **29**, 705 (1979).

[14] R. Taboryski, Ph.D. thesis, University of Copenhagen, NBI, 1992.

[15] R. L. Anderson, Solid-State Electronics **5**, 341 (1962).

[16] C. Weisbuch and C. Vinter, *Quantum semiconductor structures, fundamentals and applications* (Academic Press, New York, 1991).

[17] M. Hatzakis, in *Nanolithography: A borderland between STM, EB, IB, X-ray lithographies*, edited by M. Gentili, C. Giovannella, and S. Selci (Kluwer Academic Press, Dordrecht, 1994), pp. 13–23.

[18] K. Ensslin and R. Schuster, in *Quantum Dynamics of Submicron Structures*, edited by H. A. Cerdeira, C. Kramer, and G. Schön (Kluwer Academic Publishers, Dordrecht, 1995), pp. 247–261.

[19] R. R. Gerhardts and V. Gudmundsson, Solid State Comm. **67**, 845 (1988).

[20] L. D. Landau and E. M. Lifshitz, *Quantum Mechanics* (Pergamon Press, London, 1958).

[21] A. L. Fetter and J. Walecka, *Quantum theory of many-particle systems* (McGraw-Hill, New York, 1971).

[22] E. K. U. Gross, E. Runge, and O. Heinonen, *Many-Particle Theory* (Adam Hilger, Bristol, 1991).

[23] J. D. Jackson, *Classical Electrodynamics*, 2nd ed. (John Wiley & Sons, New York, 1975).

[24] D. Heitmann and J. P. Kotthaus, Physics Today **46**, 56 (1993).

[25] C. Cohen-Tannoudji, B. Diu, and F. Laloë, *Quantum Mechanics Vol. 1* (John Wiley & Sons, New York, 1977).

[26] P. Nozierès, *Theory of Interacting Fermi Systems* (Addison Wesley, Reading, Massachussets, 1997).

[27] J. Mathews and R. L. Walker, *Mathematical method in physics* (W. A. Benjamin, inc., Menlo Park, California, 1970).

[28] C. Steinebach, Master's thesis, University of Hamburg, Hamborg, 1996.

[29] J. Dempsey and B. I. Halperin, Phys. Rev. B **47**, 4662 (1993).

[30] N. W. Ashcroft and N. D. Mermin, *Solid State Physics* (Saunders College Publishing, Fort Worth, 1976).

[31] V. Gudmundsson and R. Gerhardts, in *Proceedings of the 15th nordic semiconductor conference*, edited by S. Franssila and R. Paananen (VTT, Espoo, Finland, 1992).

[32] C. Dahl, Phys. Rev. B **41**, 5763 (1990).

[33] V. Gudmundsson and R. Gerhardts, Phys. Rev. B **43**, 12098 (1991).

[34] R. Peierls, *Surprises in Theoretical Physics* (Princeton University Press, Princeton, New Jersey, 1979).

[35] S. A. Mikhailov and V. A. Volkov, Phys. Low-Dim. Struct. **1**, 31 (1994).

[36] W. Kohn, Phys. Rev. **123**, 1242 (1961).

[37] D. Pines, *Elementary excitations in solids* (W. A. Benjamin, inc., New York, 1977).